May 2018

# Study of Separator Damage Effects on Lithium Ion Battery Cell's Performance

Mason Pingel
*University of Wisconsin-Milwaukee*

# STUDY OF SEPARATOR DAMAGE EFFECTS ON LITHIUM ION BATTERY CELL'S PERFORMANCE

by

Mason Todd Pingel

A Thesis Submitted in

Partial Fulfillment of the

Requirements for the Degree of

Master of Science

in Engineering

at

The University of Wisconsin-Milwaukee

May 2018

# ABSTRACT

## STUDY OF SEPARATOR DAMAGE EFFECTS ON LITHIUM ION BATTERY CELL'S PERFORMANCE

by

Mason Todd Pingel

The University of Wisconsin-Milwaukee, 2018
Under the Supervision of Dr. Ilya V. Avdeev

In the world of energy storage technology, Lithium Ion batteries are considered to be among the most efficient in terms of energy- and power density. However, many consumers are fearful of the potential dangers involved in using this technology. One approach to improving the battery's safety is to focus on design of the cell itself. The separator seems to be the obvious choice in a quest to improve its safety since alterations to the other components of a battery could easily compromise the efficiency of the cell. The methods herein provide experimental results and insights that could be used to optimize the safety and efficiency of the battery's separator under various damage conditions.

# TABLE OF CONTENTS

**LIST OF FIGURES.....vi**

**LIST OF TABLES.....vii**

**ACKNOWLEDGEMENTS.....ix**

**CHAPTER 1.....1**

**1.) Introduction.....1**

1.1) Motivation and Objectives.....1

1.2) Literature Review.....5

1.2.1) Li-Ion Separator Material Properties.....5

1.2.2) Testing Apparatus.....7

1.2.2.1) Instron 5985.....7

1.2.2.2) 3-D Optical Contour Microscope.....8

1.2.2.3) SEM Imaging.....8

1.2.2.4) Mercury Intrusion.....9

1.2.2.5) Arbin.....9

1.2.3) Previous Li-Ion Battery Short Tests.....10

**CHAPTER 2.....12**

**2.) Porosity of Battery Separator.....12**

2.1) Inducing Stress onto Separators.....12

2.1.1) Compression of Separators.....12

2.1.2) Thermal Abuse on Separators.....14

2.2) Imaging on Separators.....17

2.2.1) 3-D Optical Contour Microscope-Separator Thickness..17

2.2.2) SEM Imaging - Pores Shape & Porosity.....25

2.2.3) Discussion of Results.....33

2.3) Mercury Intrusion.....36

2.3.1) Setup and Procedure.....36

2.3.2) Mercury Intrusion Failed Tests.....39

2.3.3) Mercury Intrusion Results.....42

2.4) Thermal Shrinkage.....45

2.4.1) Setup and Procedure.....46

2.4.2) Thermal Shrinkage Results.....47

2.5) Discussion of Results.....49

**CHAPTER 3.....50**

**3.) Effect of Stress on Separator on Battery Capacity.....50**

3.1) Coin Cell Testing with Damaged Separators.....50

3.1.1) Experimental Approach.....51

3.1.2) Cycling Results.....52

3.2) Experimental Results and Discussion.....54

3.2.1) Baseline vs. 34MPa.....56

3.2.2) 1st vs. 20th Cycle Discharge Capacities.....58

3.2.3) 67MPa vs. 110°C.....59

**CHAPTER 4.....61**

**4.) Effect of Porosity on Thermal Output of Battery.....61**

4.1) Pouch Cell Testing with Damaged Separators.....61

4.1.1) Experimental Approach.....64

4.1.1.1) Pouch Cell Construction.....64

4.1.1.2) Pouch Cell Cycling.....65

4.1.2) Thermal Results.....66

**CHAPTER 5.....68**

**5.) Warm Separator Subject to Compressive Stress.....68**

5.1) Separator Subject to Heat and Compression.....68

5.1.1) Experimental Approach.....68

5.1.2) Results.....69

5.1.3) Discussion.....71

**CHAPTER 6.....73**

**6.) Conclusions.....73**

6.1) Summary.....73

6.2) Conclusions.....73

6.3) Future Work.....74

**References.....76**

# LIST OF FIGURES

Figure 1: Lithium Ion Cell During Discharge……3

Figure 2: Rolls of Celgard 2325 Separator……7

Figure 3: Separator Setup Between Two Flat Plates Using Instron 5985……14

Figure 4: Hot Plate With Thermal Couple……16

Figure 5: Cylindrical Cell(a) With Battery Pack(b)……16

Figure 6: Epoxy Setup……18

Figure 7: Grinding of Cylinder……18

Figure 8: 3-D Microscopy Cross-Section of 34MPa Separator……19

Figure 9: 3-D Microscopy Cross-Section of 67MPa Separator……20

Figure 10: 3-D Microscopy Cross-Section of 101MPa Separator……21

Figure 11: 3-D Microscopy Cross-Section of 135MPa Separator……22

Figure 12: 3-D Microscopy Cross-Section of 110°C Separator……23

Figure 13: 3-D Microscopy Cross-Section of 135°C Separator……24

Figure 14: Mounted Samples For SEM Imaging ……26

Figure 15: SEM Image of Celgard 2325 Separator……27

Figure 16: SEM Image of 34MPa Separator……28

Figure 17: SEM Image of 67MPa Separator……29

Figure 18: SEM Image of 101MPa Separator……30

Figure 19: SEM Image of 135MPa Separator……31

Figure 20: SEM Image of 110°C Separator……32

Figure 21: SEM Image of 135°C Separator……33

Figure 22: Demonstration of “Iceberg” Pore……35

Figure 23: Tri-Layered Porosities of Celgard 2325……35

Figure 24: Mercury Intrusion Machine……37

Figure 25: Penetrometer……38

Figure 26: Penetrometer And Sample After Low Pressure Analysis……39

Figure 27: 34MPa Cumulative Volume vs. Pore Diameter ……40

Figure 28: 101MPa Cumulative Volume vs. Pore Diameter ……41

Figure 29: Dark Grey Patch On Separator ……42

Figure 30: Cumulative Volume vs. Pore Diameter ……44

Figure 31: Incremental Volume vs. Pore Diameter……45

Figure 32: Sample Before And After Thermal Stress……47

Figure 33: Thermal Shrinkage Graph……48

Figure 34: Diagram Of Coin Cell Using 2325 Separator……51

Figure 35: Discharge Capacity Comparison……54

Figure 36: Discharge Capacity Comparison Excluding 135MPa and 135°C……56

Figure 37: Baseline vs. 34MPa Discharge Capacity Comparison……57

Figure 38: 67MPa vs. 110°C Discharge Capacity Comparison……60

Figure 39: Thermal Camera Setup……63

Figure 40: Template For Pouch Cell Construction……65

Figure 41: Mercury Intrusion Compressed vs. Heated And Compressed……70

Figure 42: Incremental Pore Volume vs. Pore Diameter, Compresses vs. Heated and Compressed……71

# LIST OF TABLES

Table 1: Energy and Power Density Amongst Popular Batteries ……..2

Table 2: Separator Thicknesses……25

Table 3: SEM Separator Porosities……34

Table 4: Number Of Test Runs For Each Stress……40

Table 5: Mercury Intrusion Porosities……43

Table 6: Thermal Shrinkage Results……48

Table 7: Coin Cell Cycling Setup……52

Table 8: Coin Cell Testing Overview ……52

Table 9: Pouch Cell Formation And Cycling ……66

Table 10: Peak Temperatures of Pouch Cells With Stressed Separators…….67

# ACKNOWLEDGEMENTS

Firstly, I would like to thank Dr. Ilya Avdeev for allowing me to be apart of his endeavor to improve upon Lithium Ion batteries. I cannot express the amount of gratitude I have towards Alex Francis and Josh Harris, their continuous guidance, knowledge, and willingness to help me whenever I needed it made this whole project possible. I would not be giving the amount of help Dr. Ben Church gave me justice if I did not single him out as well, he was always there to bounce ideas off of and provide feedback. I also want to thank Doug Wicker, Mehdi Gilaki, Caleb Abegglen, Huainan Qu, Dr. Sobolev and lab, Dr. Qu and lab, Dr. Hardcastle and lab, and the rest of Dr. Church's lab.

Thank you to Johnson Controls for putting value in the research conducted at the University of Wisconsin-Milwaukee and sponsoring this project. Not only the funding made available, but the openness and willingness to provide materials for research is much appreciated.

Finally, I would like to thank my family for providing the support and encouragement to make this project possible. To my mom, Donna, and my dad, Todd, thank you for giving me the opportunities to pursue my interests. To my brother, Troy, thank you for instilling a competitive thirst for knowledge in the hopes of one day being as smart as you. Lastly, I want to thank my girlfriend Lindsay who made many sacrifices to help me accomplish my research goals. Whether it was picking me up late at night from school or watching our dog, Bert, Lindsay did whatever she could to help me finish this study.

# CHAPTER 1. Introduction

## 1.1) Motivation and Objectives

The world today is facing a crisis of cataclysmic proportions known as global warming. Carbon Dioxide is being released into the atmosphere at a steadily increasing pace from the burning of fossil fuels, causing a greenhouse effect [1]. Now more than ever, other forms of clean energy need to be researched and improved upon to be a sustainable source of energy. Lithium Ion (Li-Ion) batteries give ability to store this clean energy and discharge it at a high enough current to power anything from a cellphone to an electric car [2]. Improving upon this technology could aid in the world's quest to move to cleaner energy and in turn make earth habitable for generations to come.

Along with the environmental motivation of this project is also the motivation to make Lithium Ion battery cells safer. In the past, Lithium Ion cells have posed a fire hazard and are not generally known as the safest type of battery [3]. Samsung phone and tablets caught media attention when batteries would heat up to the point in which they started to combust causing user injuries [4, 5]. Not only do Li-Ion cells pose a threat to phone and other small electronics' safety, but they can also be extremely dangerous inside of electric vehicles. Combustion in electric vehicles has been known to happen after a collision [6, 7]. Finite element modeling conducted by Trattnig and Leitgeb captured the stress induced by a car collision causing thermal runaway that ignites an electric car fire [8]. Although these thermal runaway cases are rare, any improvement to the cell in which it creates a

safer final product for the user without compromising the cell's efficiency is a welcomed addition. This "efficiency" in terms of energy density and power density is what intrigues researches most about Lithium Ion batteries. Table 1 shows the comparison of Lithium Ion versus other mass-produced battery types.

| **Battery Type** | **Lead Acid** | **Ni-Cd** | **Ni-MH** | **Lithium Ion** |
|---|---|---|---|---|
| Energy Density (Wh/kg) | 35 | 40-60 | 60 | 120 |
| Power Density (W/kg) | 180 | 150 | 250-1000 | 1800 |

Table 1: Energy and Power Density Amongst Popular Batteries [9]

Lithium Ion battery cells consist of an anode, cathode, separator and an electrolyte solution. The cell used over the duration of this study was a graphite anode, and a nickel manganese cobalt cathode. The electrolyte solution used during this project was a Lithium Hexafluorophosphate ($LiPF_6$) solution dissolved in organic solvents in which ions transfer between the anode and cathode [10]. The separator used was the Celgard 2325, a tri-layered separator consisting of a Polyethylene (PE) layer sandwiched in between two Polypropylene (PP) layers. The main purpose of the separator is to prevent contact between the anode and the cathode [11]. Batteries, including Lithium Ion batteries, use chemical reaction, which energy is converted into electrical energy. The ions pass from cathode to anode through the separator and the electrons pass through a circuit to transfer from anode to cathode during discharge, the charging process is the reverse of the

discharge process by exerting electricity into the cell [12]. The discharge stage of the battery's cycle is depicted in Figure 1 [9].

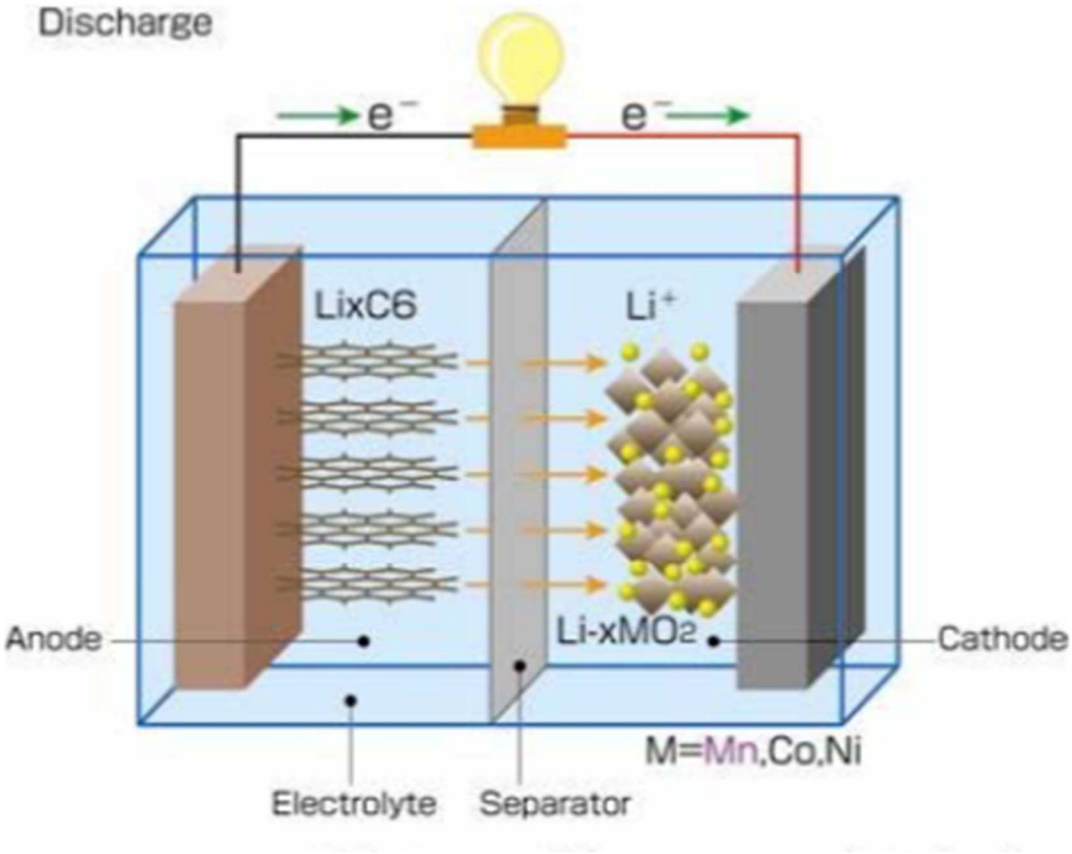


Figure 1: Li-Ion Cell During Discharge [9]

When attempting to improve safety on a Lithium Ion battery, one can either improve safety outside the cell, or improve safety inside of the cell. Examples of outward safety improvements may be a battery case, housing unit, dampeners in between the cells, etc. These outward safety improvements can be somewhat large, in an industry that values the efficiencies of high energy density, outward safety improvements seem counterproductive. Inward safety improvements would be

improvements such as using a different electrolyte solution, improving the anode/cathode, or improving the safety of the separator. Although changes to the anode or cathode are possible, it would be difficult to make changes without compromising the efficiency of the cell. The same is true for the electrolyte, changes and improvements are possible, but it seems unlikely to improve the safety of the battery while improving the abilities of the cell with that approach. For example, a more "watered down" electrolyte could be used that contained less lithium, this would make the electrolyte less reactive and potentially more safe, but would compromise some of the power output of the battery. Some safety measures are already implemented inside of the separator, such as the automatic shutdown of the separator, and improvements seem possible. The separator was chosen as the focus of the study since it was deemed the most influential safety component inside of the battery cell due to it's ability to close it's pores effectively shutting off the battery when needed.

The main goal of this project was to create a better understanding of the impact that a battery separator has on a battery cell. More specifically, the study was to observe the effect that a damaged, but not destroyed, separator plays on a battery cell. The approach was to isolate the separator by damaging it before it was placed in a cell. By only damaging the separator in any tests, any new effects on the battery could then be attributed to the damaged separator. Testing would first be conducted on the separator by itself, then after attributes were observed of the separator, the damaged separator would then be inserted into an otherwise healthy cell to observe the effects the separator had on the cell as a whole.

## 1.2) Literature Review

The following machines were either used in this study to impose a stress upon the separator or to observe the separator and/or it's effect on the battery cell. The separator itself is also briefly discussed in order to establish the known attributes of the separator in which the damaged separators were compared to.

### 1.2.1) Lithium Ion separator material properties

The Celgard 2325 separator layer is one of the most widely used separators made by Celgard, it is a tri-layer separator composed of both Polyethylene (PE) and Polypropylene (PP) [13]. There are two different manufacturing methods utilized to produce battery separators, termed wet and dry manufacturing. In wet manufacturing, a polyolefin resin is mixed with a hydrocarbon and heated until it is melted, the mixture is then extruded as a sheet to form micropores [13, 11]. In dry manufacturing, the polyolefin is brought to it's melting point in which it is extruded and then annealed, after it is annealed, it is extruded again which creates linearly aligned, small, micropores [13, 11]. The Celgard 2325 separator is manufactured using the dry process to create a separator with linearly aligned micropores [14]. These pores are what the lithium ions pass thru from either the anode to the cathode, or cathode to the anode depending on if the battery is charging or discharging [15]. The pores of the separators are engineered to close at the materials melting temperature so that the separator can automatically shutdown the battery before it reaches a thermal runaway [13]. This shutdown occurs at about 130°C which is a slightly lower temperature than Celgard 2325's melting point at

135°C [14]. A study conducted by Avdeev et al determined that an increase in temperature to the tri-layered polyethylene polypropylene separator significantly decreases the strength of the material [16]. Ideally, a separator should have a high porosity and be very thin to safe space and reduce internal resistance, however, if the porosity is too great or the separator is too thin, there runs a greater risk of an internal short [17]. The Celgard 2325 has a porosity of 40±1% and is 25μm thick [13]. Porosity is calculated using Equation 1 [14]. A study by Gilaki et al determined that the separator and other parts of the battery's material properties do not change significantly with or without the presence of the battery's electrolyte [18], showing that tests done to a dry separator should be sufficient in demonstrating mechanical damage in a live battery. Figure 2 shows the rolls of 2325 separator material that Celgard sells.

$$\text{Porosity (\%)} = \left[1 - \frac{\left(\frac{sample\ weight}{sample\ volume}\right)}{polymer\ density}\right] \times 100 \quad (1)$$

Figure 2: Rolls of Celgard 2325 Separator

1.2.2) Testing Apparatus

In order to properly observe the effects that a damaged separator has on a battery cell, damaged separators and their effects needed to be compared to undamaged separators. The following apparatus were employed to either impose a stress on or observe the effects on a battery separator or a battery cell.

1.2.2.1) Instron 5985

The Instron 5985 tensile testing machine is chosen to inhibit tension or compression on the material. It is chosen for these tests because of it's accuracy as well as the amount of force it can output. The measurements are fine enough to

obtain hardness tests on a piece of tofu [19] and the force is strong enough to compress 250kN of force.

1.2.2.2) 3-D Optical Contour Microscope

A 3-D Optical Contour Microscope gives magnified images of a sample in three dimensions while most microscopes only view in two dimensions. 3-D Optical Contour Microscopes are different because they can view three dimensions, this is possible because 3-D Optical Contour Microscopes take two images at an angle through a refractive mirror creating the depth dimension [20]. Along with the other X and Y dimension that normal optical microscopes can see, the Z directions is available using the afore mentioned method.

1.2.2.3) SEM imaging

Scanning Electron Microscopy (SEM) imaging is a useful tool to obtain a magnified image for characterization of a sample. These images have been used to observe a variety of materials, for example, SEM imaging has been used to observe pore size, pore shape, porosity, surface roughness, etc. of PVDF-based polymeric membranes [21]. As well as being used to actually observe a battery separators pores before and after it had been compressed [18]. With power of magnification, it was determined that SEM imaging could accurately determine separator thickness as well as give a basic understanding of the separator material's porosity and pore sizes.

1.2.2.4) Hg Intrusion

Mercury Intrusion is a procedure used to find the porosity of a variety of porous materials. Usually used in larger sized pore materials such as asphalt or cement [22], Mercury Intrusion is not normally the first choice for smaller pored materials. However, in the case of a polyethylene, polypropylene material such as a battery separator, Mercury Intrusion was deemed a better option than a liquid nitrogen test, which is also used to determine porosity in a substance, due to fear of the Polyethylene-Polypropylene separator reacting with the nitrogen due to the extremely cold temperatures. Mercury Intrusion has been used in the past to measure the porosity of similar lithium ion separators as in tests conducted by, researchers Aurora et. al, Dijan et. al, Huang, Song et al, and Ryou et al [14, 23, 15, 24, & 25].

1.2.2.5) Arbin BT-2000

The Arbin BT-2000 is a testing machine generally used to run small battery cells such as a coin cell or a pouch cell. Arbin battery cyclers can control the voltage and current as well as record performance data from the battery cell that it is cycling. Little research has been conducted using altered battery separators and an Arbin other than a study conducted by Wang et al to observe the overcharging of a battery and the protection from an electroactive polymer composite separator in a lithium ion battery [26]. Other than potential improvements to separators, such as the overcharge protection study, the opportunity exists to study battery cycling with isolated damage of internal components like the separator.

1.2.3) Previous Li-Ion Battery Short Tests

Lithium Ion battery testing, characterization, and simulation work up to this point has included the following research efforts. These tests can be characterized into either thermal, electrical or mechanical abuse tests [27]. Considering thermal abuse, and electrical abuse tests are abuses containing many outside factors, it was determined that mechanical abuse would be the best option to focus on. The vast majority of these tests have been conducted on a complete battery so that all of the components of the battery are affected. Such testing was utilized by Sarhaei et al when they compressed completed pouch cells (some while the cell was cycling) and made observations about the cell [28]. Although this method almost assures a failure, it does not isolate single battery component, making the effort more difficult to determine the source of failure. This strategy makes it difficult to analyze batteries that are weakened but not completely failed since many of these tests are to observe catastrophic failure.

Catastrophic failures can occur from the onset of an internal short circuit [27, 29, 31, 30]. In a study conducted by Kim et al, internal shorts can be characterized into four main types; aluminum-copper short (metal of cathode-anode), copper-cathode active material short (anode-cathode active material), aluminum-anode short (aluminum touching anode, often leads to thermal runaway), and finally the cathode anode short [31]. A study conducted by Joshua Lamb and Christopher Orendorff observed a variety of shorts and the temperature increases that accompany them [30]. Observing internal shorts can be difficult due to the lack of

visual evidence inside of the battery during the short, so simulations have been made to observe the internal phenomena. Santhanagopolan et al created a model to observe four main types of internal shorts and the temperature increases accompanying them inside of the battery [32]. In the future, modeling simulations can be used to fully understand what is going on inside of a Li-Ion battery during a short, but more research on the individual components of a battery may be needed to improve the accuracy those models.

One test that can be conducted to cause a catastrophic failure is the "nail test". In a study conducted by Cheon-Soo et al, a nail penetration test is conducted to cause an immediate catastrophic failure. This test was accomplished by using a steel nail to penetrate through the anode, cathode, and separator causing an internal short and causing catastrophic failure, which created thermal runaway [31].

# Chapter 2. Porosity of Battery Separators

If a battery separator becomes too thin from mechanical deformation of a cell, possibility of a short increases because an electrical charge can jump through the separator with very little resistance [17]. To counteract this, battery separator manufacturers (in this case, Celgard) have put in a fail-safe in which the battery automatically shuts off by closing up the pores in the separator so no ions can pass through during high temperatures [13]. The following experiment investigates what happens to the pores of an undamaged separator and one that has reached a critical load or temperature to close the pores, inhibiting the electrochemical reaction from taking place.

## 2.1) Inducing Stress on Separators

Two types of stress that the separators were subject to, compressive stress and thermal stress. Tensile stresses and torsional stresses were not chosen to be observed because those types of stresses and their effects are well documented [17, 33, 13, 34, 16]. Also, tensile and torsional stresses are more likely to occur during the manufacturing process of the battery separator [16,13]. It was determined that compressive and thermal stresses were more likely to occur in an electric vehicle battery pack, for example in a car crash or an overheated situation.

### 2.1.1) Compression of Separators

The Celgard 2325 tri-layer separator was used as the material studied in this research. An Instron 5985, shown in Figure 3, was used to compress the samples.

This ensured a controlled and uniform compression. A steel template was used to maintain a repeatable 19mm by 81mm area of compression. Samples were cut slightly larger than the template (21mm by 84mm) out of larger separator sheets using an XACTO knife. After the sample was cut to the correct size, and the steel template was set in place in the Instron, the separators were compressed to 33.71MPa, 67.42MPa, 101.13MPa and 134.84 MPa. These compressive stresses were chosen after analyzing data given from a Li-Ion Cell impact testing done by Gilaki et al [35]. In Gilaki's impact testing procedure, compressive forces on the cell reached 52.0kN with internal stresses reaching 67.42MPa. To ensure accuracy, at least 10 separator samples were compressed at each stress level.


Figure 3: Separator Loading Setup Between Two Flat Plates Using Instron 5985

2.1.2) Thermal Abuse on Separators

The second type of stress that the separators were subject to was thermal stress. As stated earlier, the automatic shutdown and melting point of Celgard 2325

is at 130°C and 135°C respectively [14]. Also, 80°C is the maximum temperature the separator can handle before deformation [36]. Temperatures selected for damaging the separators were 110°C and 135°C. These temperatures were chosen because 135°C is above the automatic shutdown and 110°C is in the middle between an un-deformed separator and a melted separator. 80°C was not tested because since that is a temperature before deformation, the control at room temperature (~27°C) is assumed to be sufficient observation for that temperature.

A hotplate was chosen to melt the separators, due to the uniformity of the temperature as well as the flatness of the surface. The surface of the hotplate temperature was checked for accuracy before each thermal test using a thermocouple as seen in Figure 4. Since the hotplate has a relatively flat surface, a stainless steel plate could be placed on top of the separator sheet being melted to assure a thermal abuse that could be observed in a tightly packed Lithium Ion battery cell like the cylindrical cell shown in Figure 5. Each separator was subject to the desired thermal abuse for 3 minutes to assure a uniform temperature. The separator was subjected to the thermal stresses in larger pieces and then cut to the correct size. Again, using a template and an XACTO knife.

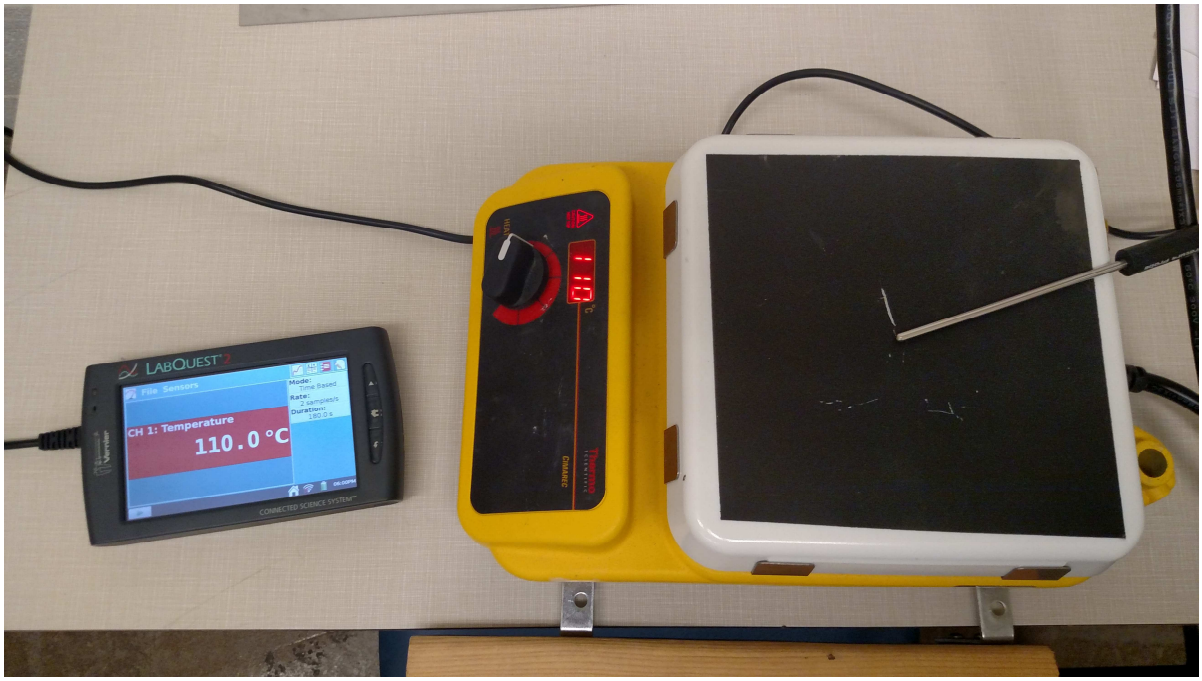


Figure 4: Hotplate with Thermal Couple

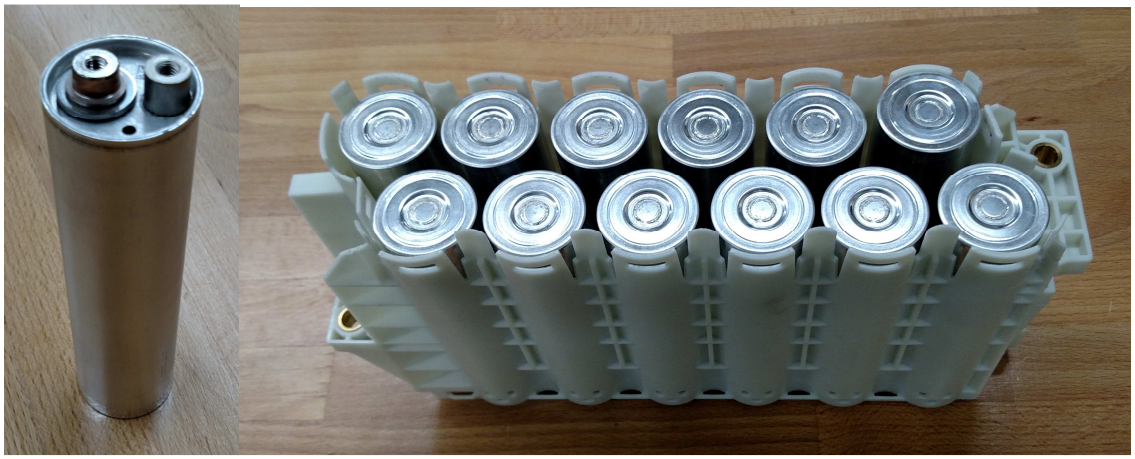

(a) (b)

Figure 5: Cylinder Cell (a) with Battery Module (b)

## 2.2) Imaging of Separators

Damage observations of the separator can be made with the naked eye such as the color or transparency of the separator. However, observations for the purpose of electrochemical performance characterization occur on the micro-scale. For this reason, SEM imaging was used to understand the shape changes of the pores, and a 3-D Optical Contour Microscope was used to measure the changes in the separators cross section.

### 2.2.1) 3-D Optical Contour Microscope - Separator Thickness

The objective of 3-D Microscopy measurement was to observe the correlation between the thickness of the separator and the porosity of the separator. The separator samples were cut to 10mm by 10mm and mounted upright in an epoxy solution for viewing the cross section under the microscope as seen in Figure 6. The epoxy was left to cure overnight, then it was polished using different abrasive levels to remove as many scratches as possible as seen in Figure 7. The epoxy cylinders were then placed under the 3-D Optical Contour Microscope to observe the samples thickness and obtain an image of the thickness of each sample as seen in Figure 8 through Figure 13. A 2-D plane from each 3-D image was chosen to observe. Using the image measurement program, ImageJ, the thickness of each separator was obtained as can be seen in Table 2.

Figure 6: Epoxy Setup


Figure 7: Grinding of Cylinder

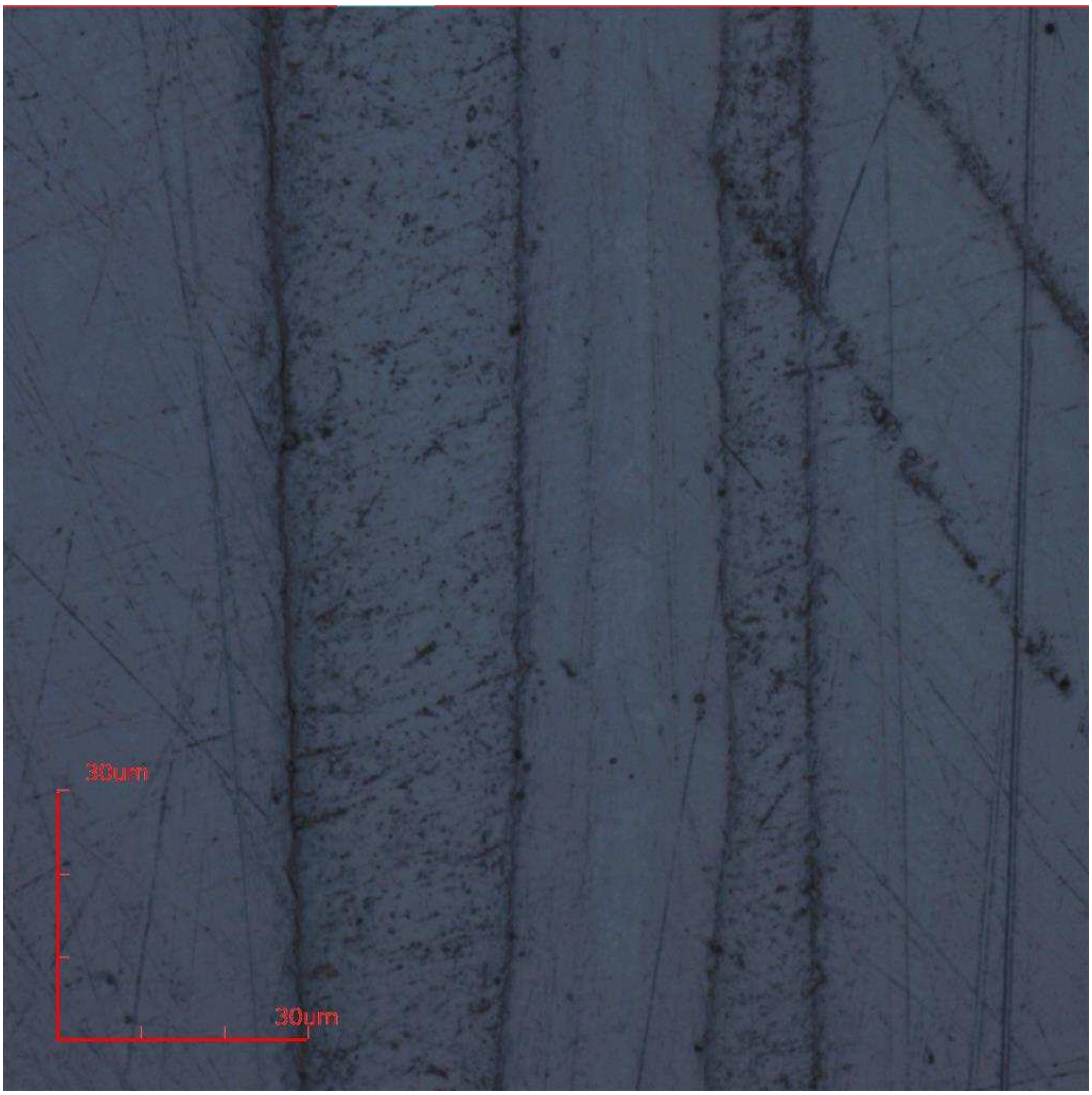


Figure 8: 3-D Microscopy Cross-Section of 34MPa Separator

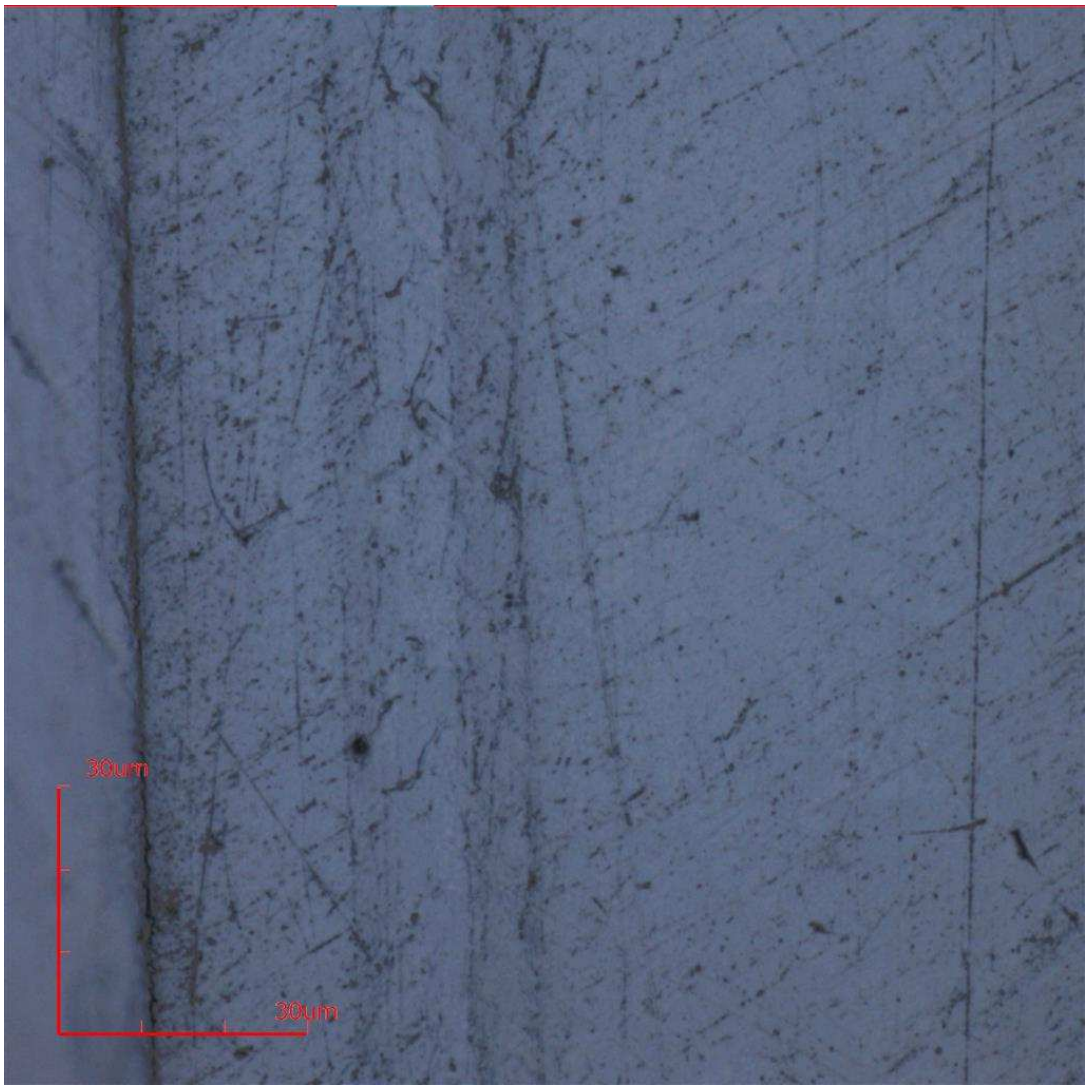


Figure 9: 3-D Microscopy Cross-Section of 67MPa Separator

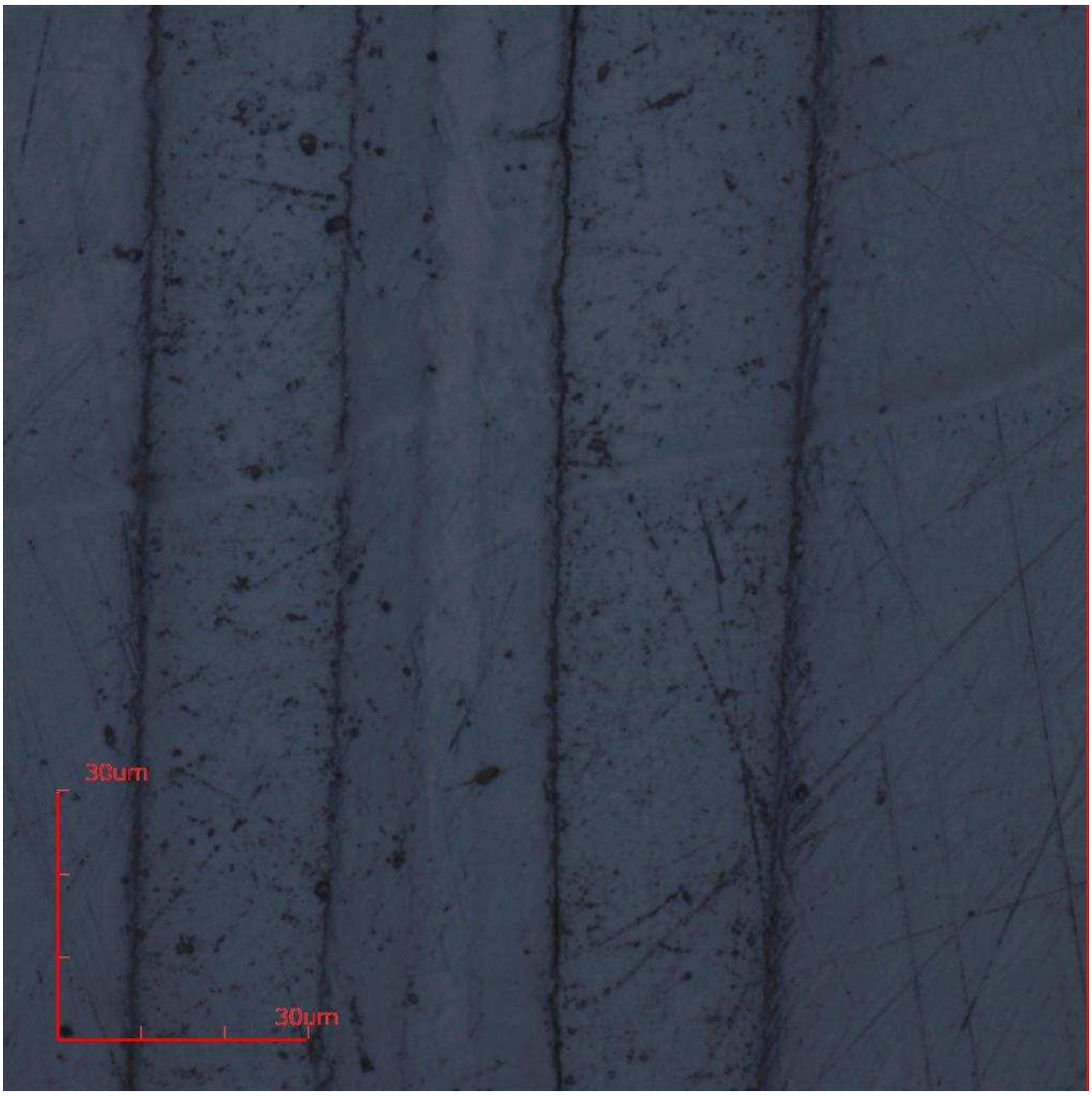


Figure 10: 3-D Microscopy Cross-Section of 101MPa Separator

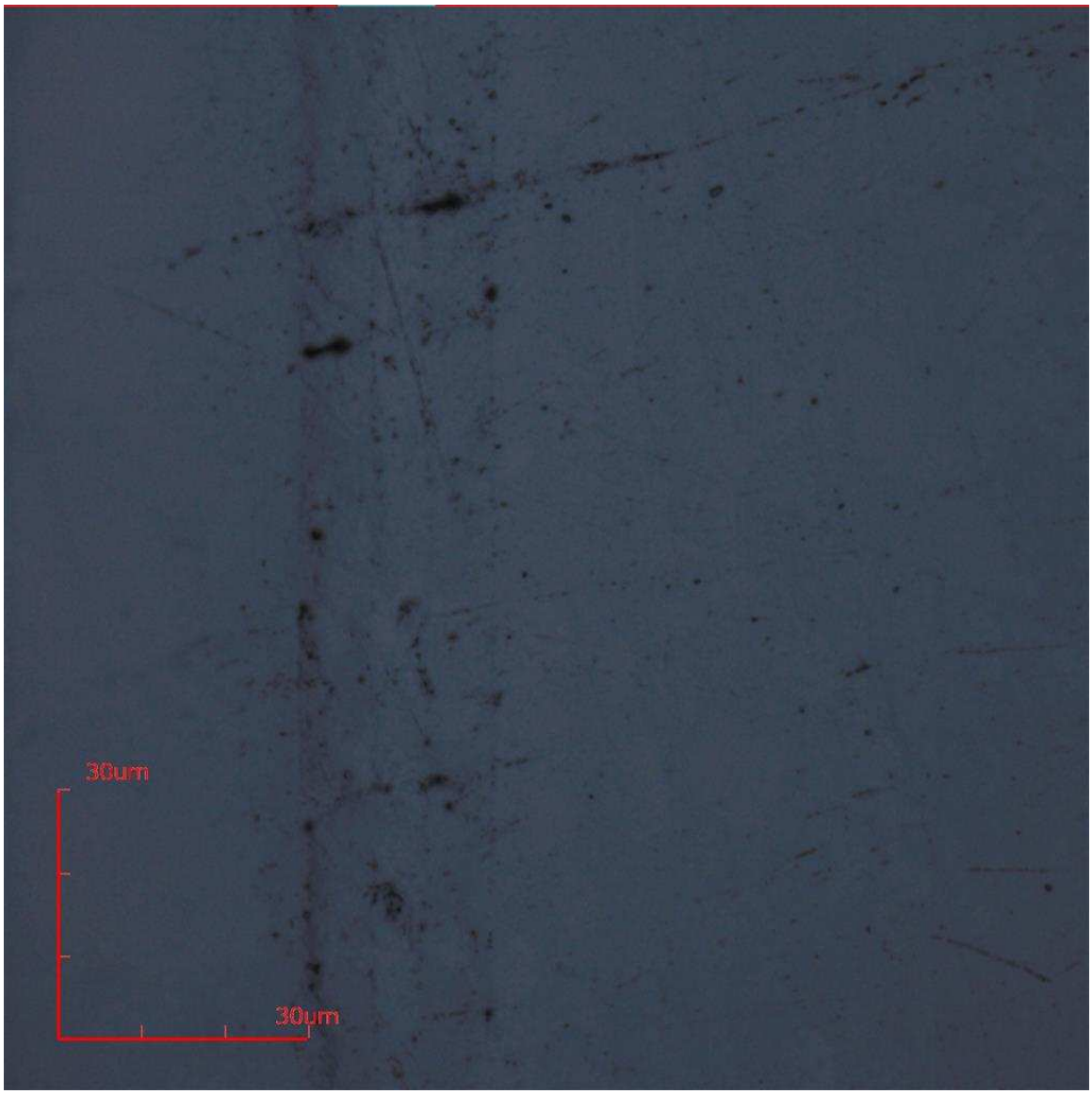


Figure 11: 3-D Microscopy Cross-Section of 135MPa Separator

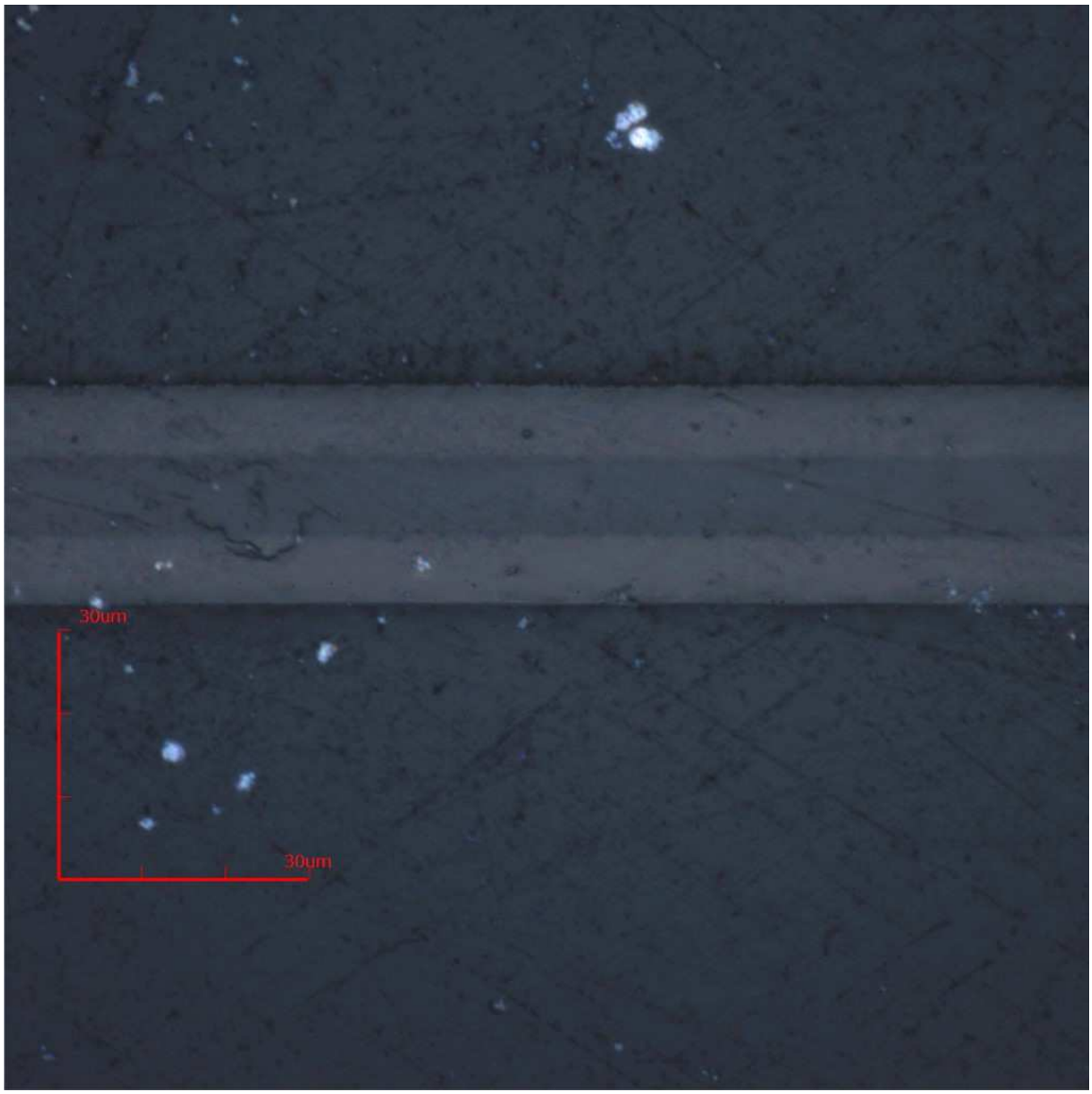


Figure 12: 3-D Microscopy Cross-Section of 110°C Separator

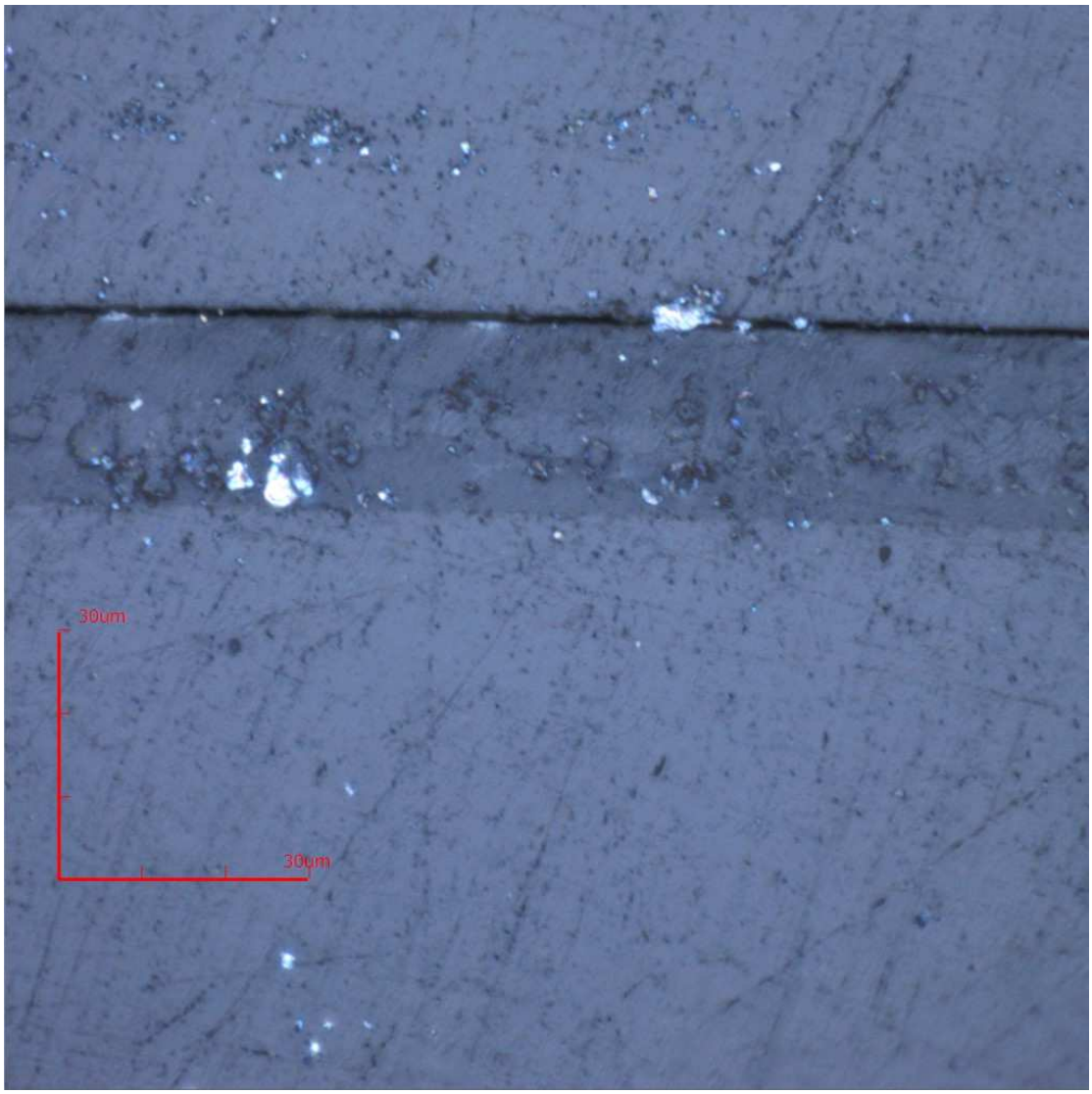


Figure 13: 3-D Microscopy Cross-Section of 135°C Separator

| Stress Level | Thickness (μm) |
|---|---|
| Undamaged | ~25.0 |
| Mechanical Loading | |
| 34MPa | 24.8 |
| 67MPa | 24.6 |
| 101MPa | 22.2 |
| 135MPa | 21.0 |
| Thermal Loading | |
| 110°C | 25.0 |
| 135°C | 22.5 |

Table 2: Separator Thickness

2.2.2) SEM Imaging - Pores Shape & Porosity

Scanning Electron Microscopy (SEM) has been used to observe battery separators in the past [14, 23, 13, 18, 33, 11, 15, 26, 37]. Many of the observations of battery separators using SEM have been to observe the separators after being subject to a tensile stress [33, 13, 11, 37]. However, as mentioned before, there have been observations taken of a separator after compression, which shows that this method can be used to find accurate results [18].

In this particular experiment, SEM imaging was used to determine the deformation of the separator pores after put under stress. After each separator was subject to a stress, segments small enough to fit inside the microscope were cut out using an XACTO knife. The separator pieces were then mounted to a steel cylinder using carbon tape as can be seen in Figure 14 and were coated with 1nm of Gold and

Iridium coating to assure conductivity3-D.  Once all pieces were mounted, the cylinder was placed in the SEM and images of each separator piece were taken and observed as can be seen in Figures 15 through 21.

Figure 14: Mounted Samples for SEM Imaging

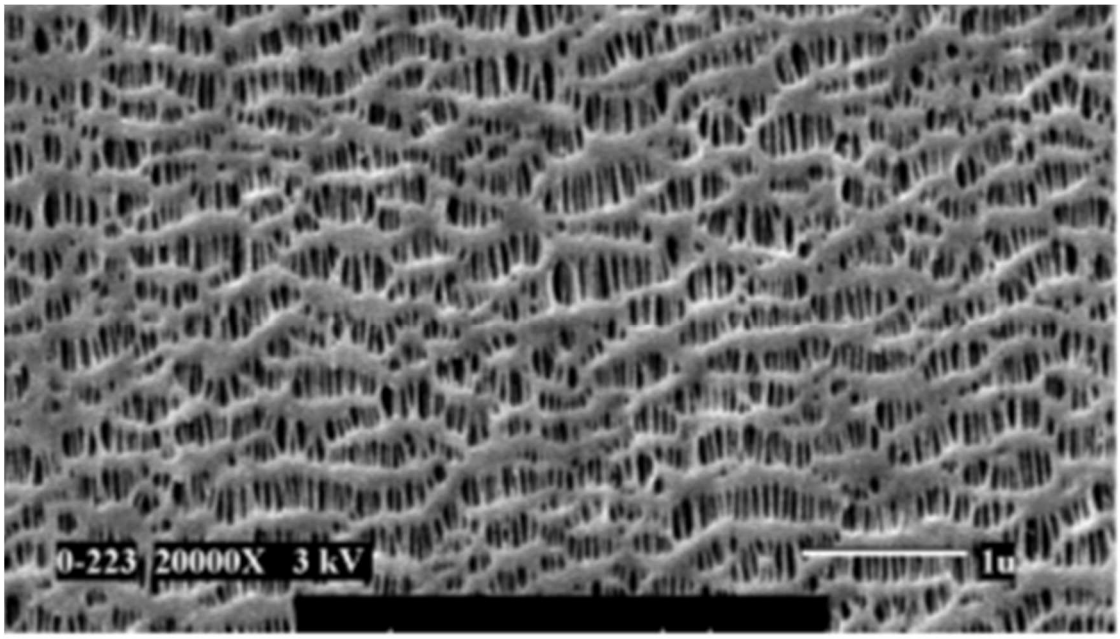


Figure 15: SEM Image of Celgard 2325 Separator [14]

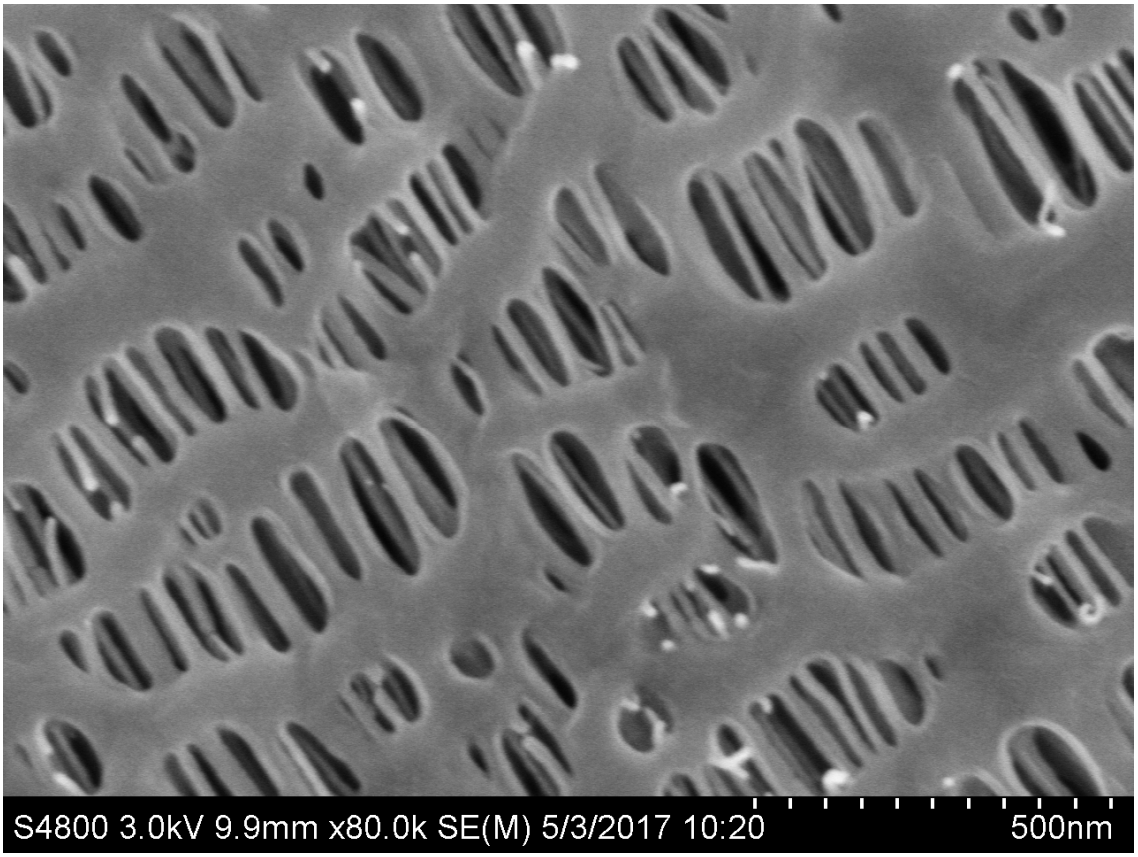


Figure 16: SEM Image of 34MPa Separator

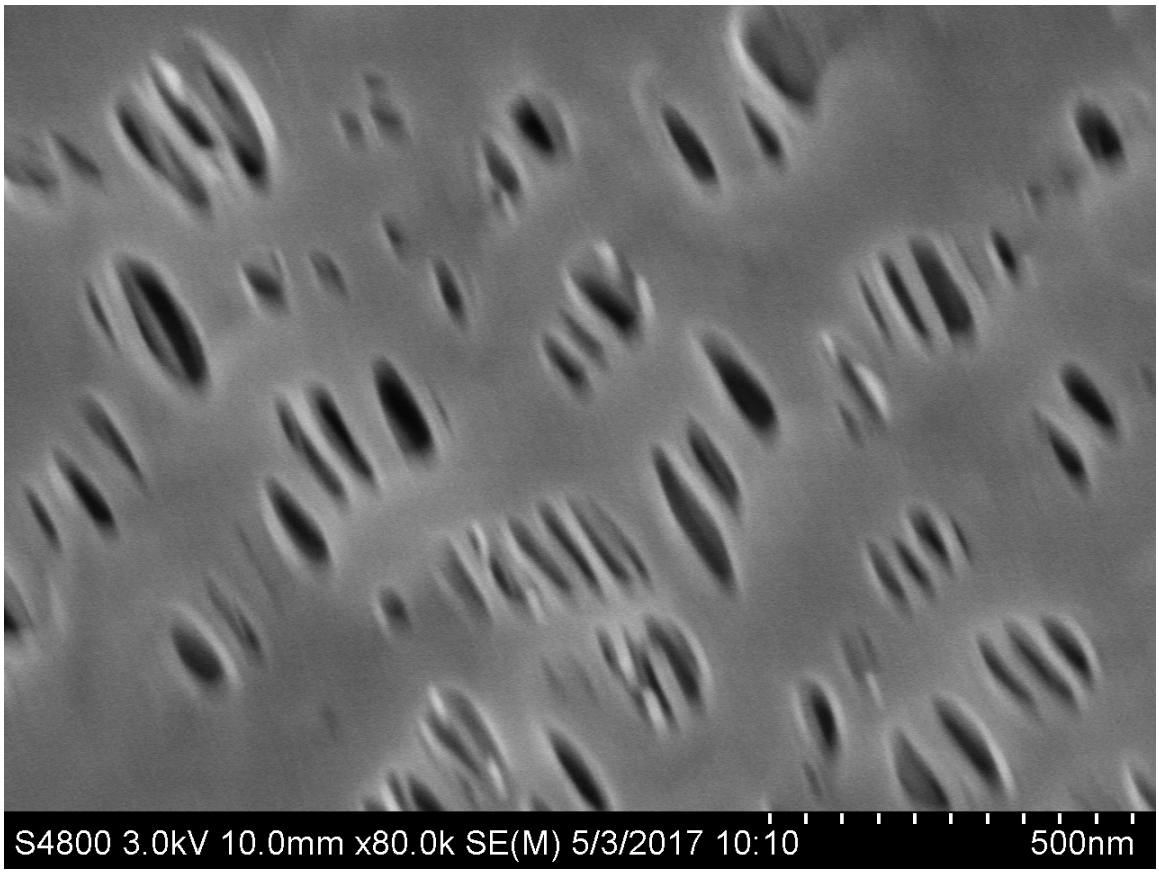


Figure 17: SEM Image of 67MPa Separator

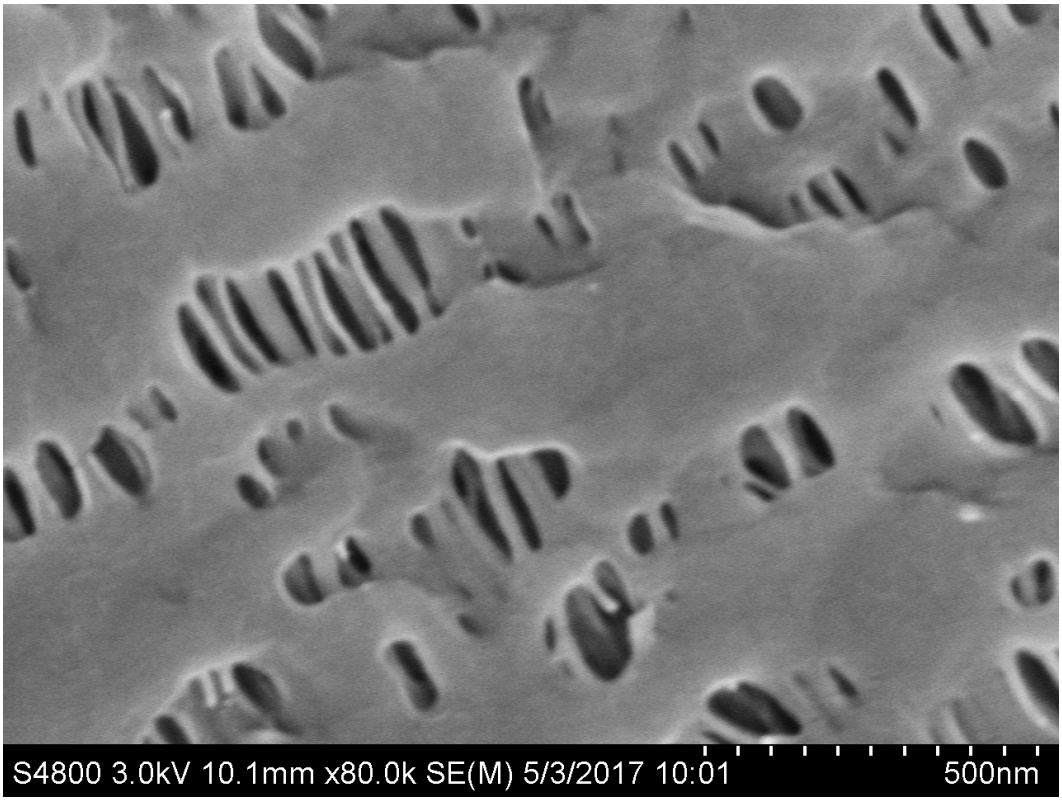


Figure 18: SEM Image of 101MPa Separator

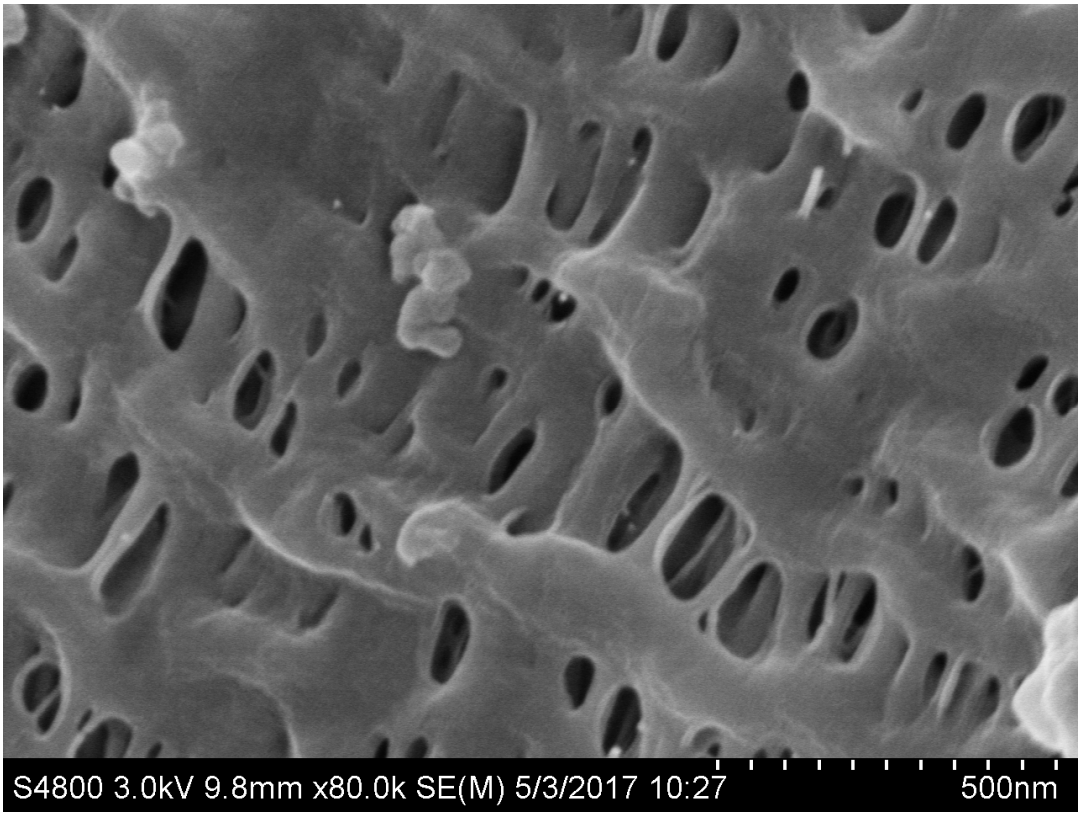


Figure 19: SEM Image of 135MPa Separator

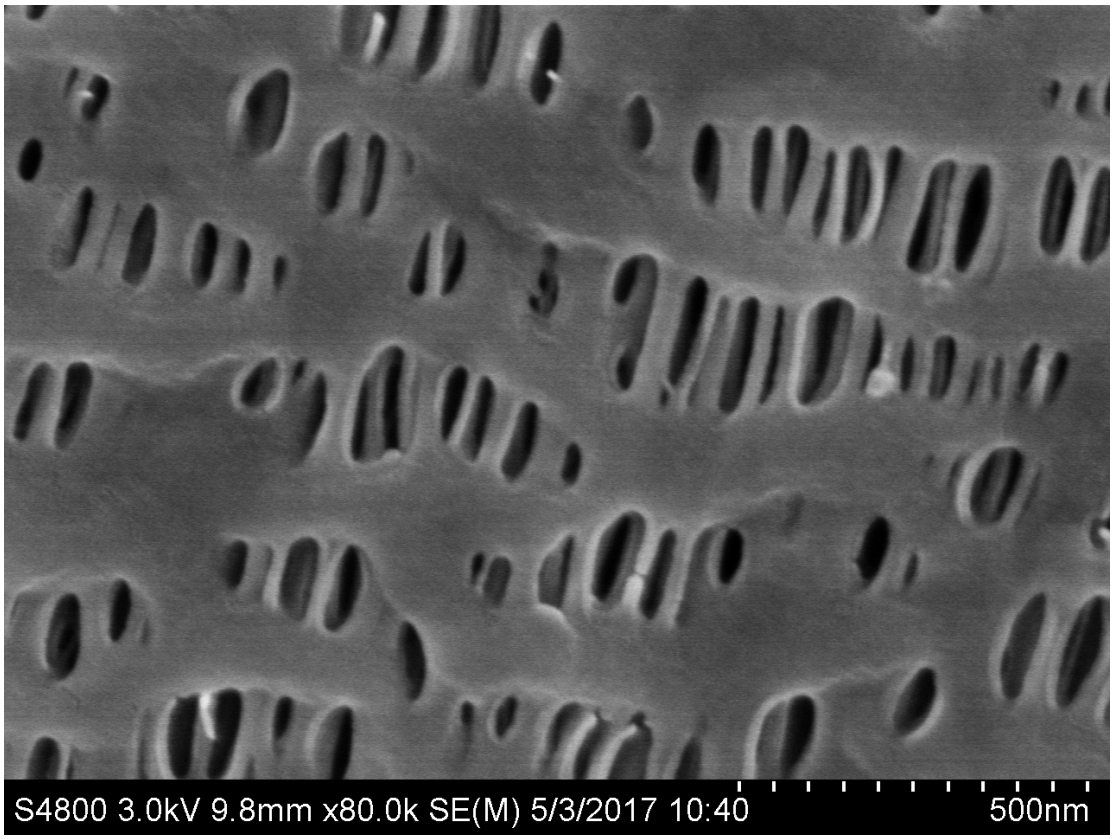


Figure 20: SEM Image of 110°C Separator

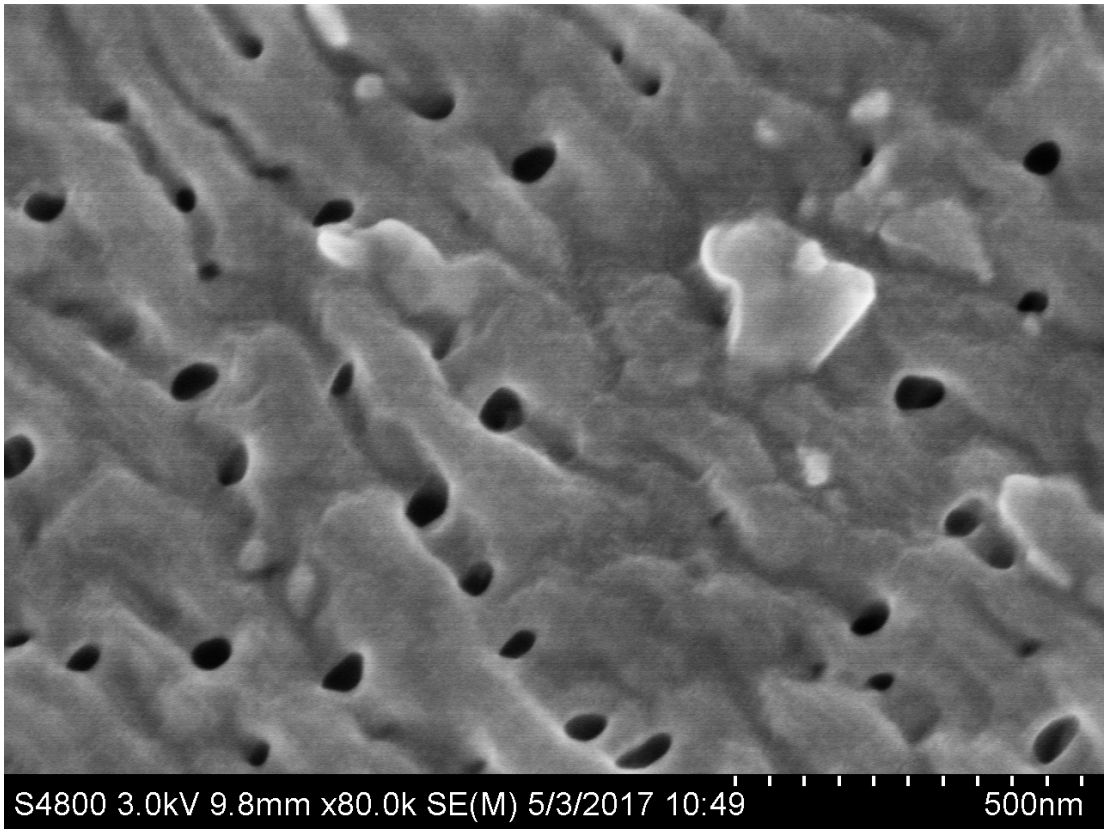


Figure 21: SEM Image of 135°C Separator

2.2.3) Discussion of Results

From the SEM images, the porosity was found for each separator using a custom Matlab program to count the pore area in the image. Images were converted to black and white, the Matlab program counted the amount of white pixels and the amount of black pixels, the black pixels were considered pores, from that the porosity for each sample was calculated. The porosity values found can be seen in Table 3. However, these values were found to be inaccurate when the baseline was compared with the known porosity of Celgard 2325. The porosity was 25% of the known value. A hypothesis of the discrepancy is that, the SEM captures a two dimensional image, it cannot take into account for pores that may expand below the

surface like and “iceberg” type pore as demonstrated in Figure 22. Another hypothesis for the discrepancy is that the separator under review is a tri-layer separator composed of two different materials [13], meaning that the different layers will have different porosities, as shown in Figure 23. Even considering the discrepancy, results from the SEM can be used to characterize the impact of stress when comparing Figures 15 through 21. These deformations could give insight to the battery performances after being subject to a stress. The separator thins when subject to a higher stress, but a correlation between the separator thickness and its porosity couldn’t be found until a correlative correct porosity reading was determined using another technique.

| **Stress** | Undamaged | 34MPa | 67MPa | 101MPa | 135MPa | 110°C | 135°C |
|---|---|---|---|---|---|---|---|
| **Porosity** | 10% | 12% | 8% | 6% | 5% | 9% | 3% |

Table 3: SEM Separator Porosities

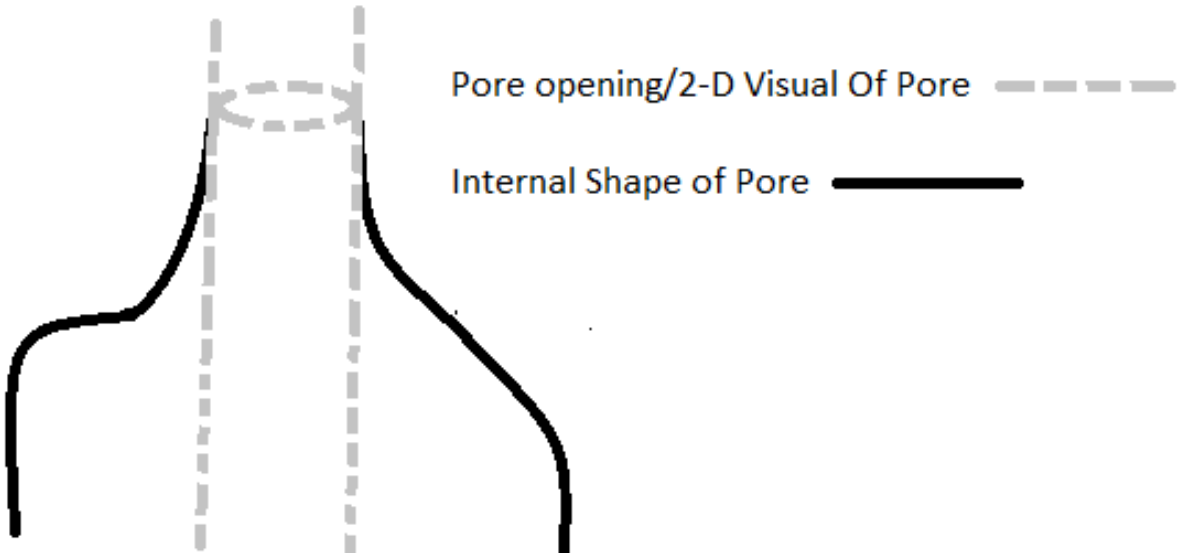


Figure 22: Demonstrations of "Iceberg" Pore

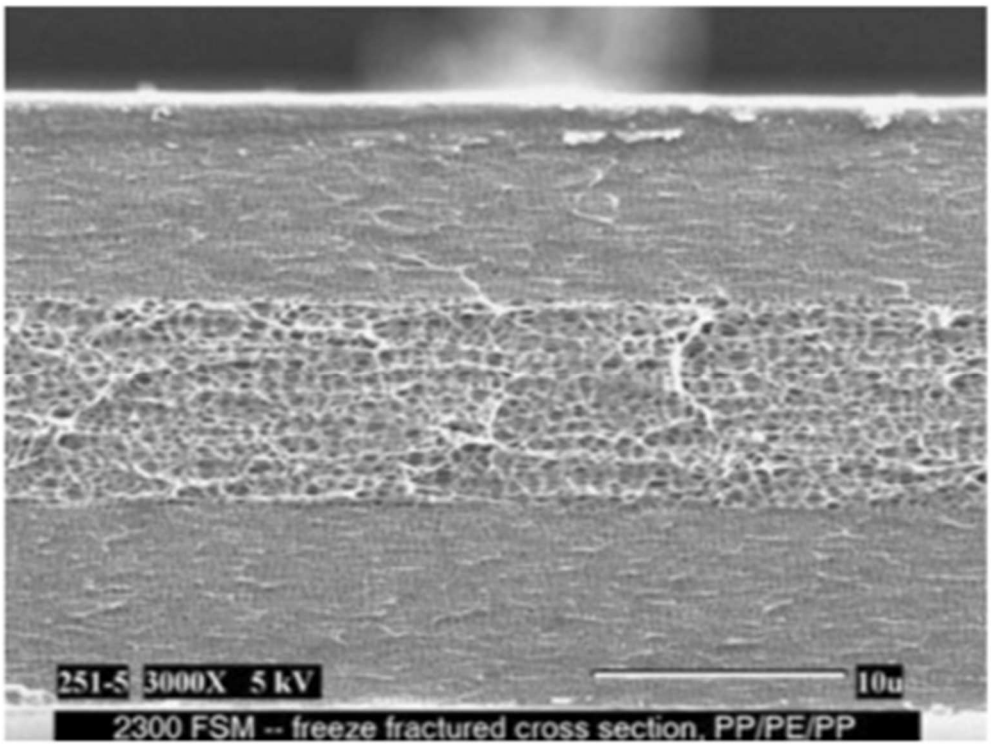


Figure 23: Tri-Layered Porosities of Celgard 2325

[14]

## 2.3) Mercury Intrusion

Mercury intrusion has been used before on separator samples to determine their porosities [14, 23, 15, 24, & 25]. Celgard 2325 would most likely be difficult to measure using this method due to its small pore size and the PP-PE-PP material makeup. To assure accuracy, results from a baseline test would be compared with the known value given by Celgard to be ~40%.

### 2.3.1) Setup and Procedure

A Micrometrics AutoPore IV 9500 Mercury Porosimeter (Figure 24) was used to conduct the mercury intrusion. The machine functions by forcing mercury into a penetrometer as seen in Figure 25. To maximize the surface area of the sample inside of the penetrometer, long thin strips of the sample (19.05mm by 80.96mm) were cut using an XACTO knife, weighed, then rolled up and placed inside of the penetrometer reservoir. Once the penetrometer is inside of the Porosimeter, the sample is subject to two different pressure analyses. The first pressure analysis is a low pressure analysis. This analysis pushes mercury into the penetrometer with a pressure slightly higher (~20psi) than atmospheric pressure, fills in the empty volume of the penetrometer and larger pores with mercury as seen in Figure 26. The filled penetrometer is then taken out of the low pressure port and weighed again. After the penetrometer is weighed, the penetrometer is placed into the high pressure port and a high pressure analysis is run. During the high pressure analysis, mercury is slowly pushed in at upwards of 52,000psi. This high pressure pushes

mercury into the smaller pores of the separator, filling the separator completely with mercury. Knowing the original weight/density of the separator, density of mercury, and the difference in mercury between the high and low pressure analyses, the machine can then calculate the remaining porosity of the sample using Equation (2). Pore diameter distribution and pore shape were determined by the AutoPore IV using the Laplace Equation (2) where R is pore radius, ΔP is the mercury pressure, γ is the surface tension equal to $480\text{x}10^{-5}\text{N}cm^{-1}$, and θ is the contact angle of 130° for all samples.

$$R = -\frac{2\gamma\cos(\theta)}{\Delta P} \qquad (2)$$


Figure 24: Hg Intrusion Machine

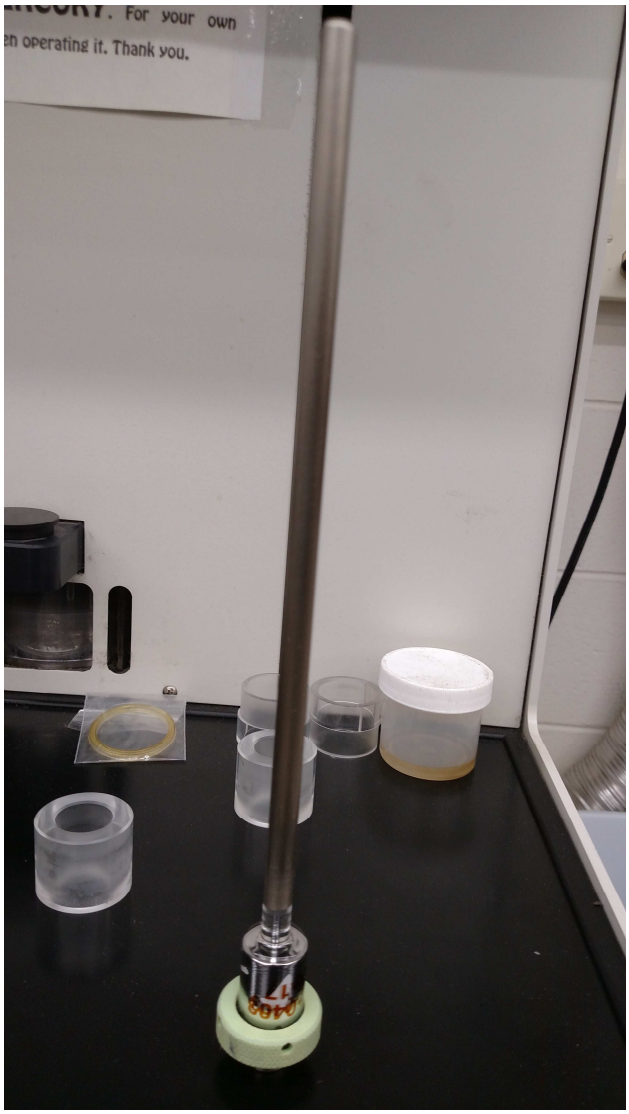


Figure 25: Penetrometer

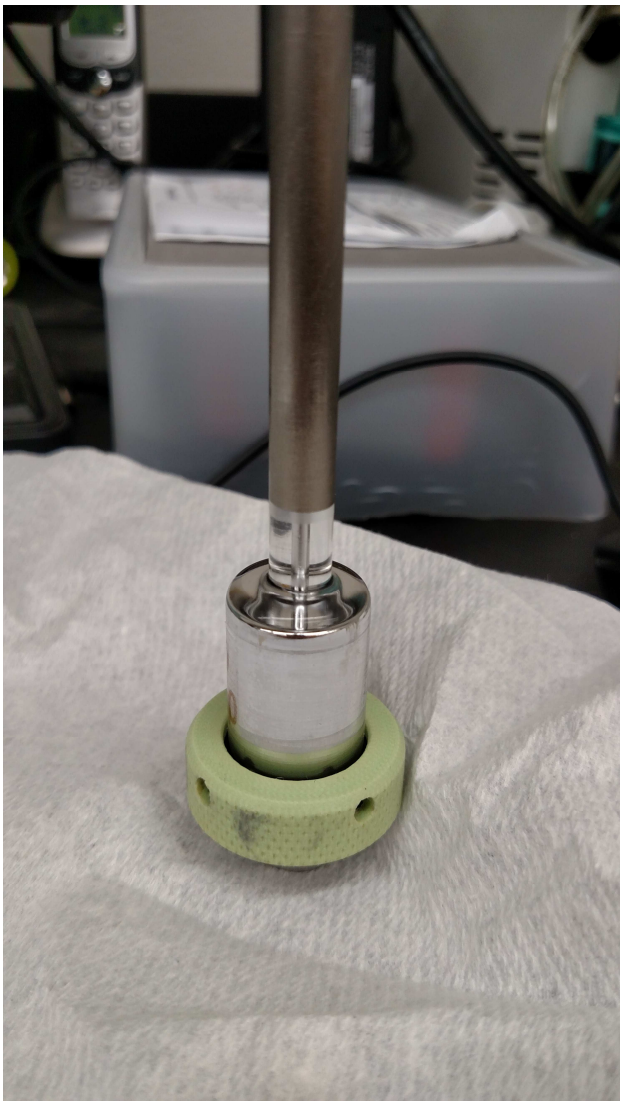

Figure 26: Penetrometer and Sample after Low Pressure Analysis

2.3.2) Mercury Intrusion Failed Tests

Each separator stress level was tested with the mercury intrusion process at least three to assure accuracy. However, some stress levels had to be tested more times than others as seen in Table 4. The 34MPa samples showed repeatability in the first three trials; see Figure 27. Tests that were repeatable for the duration of the test were deemed accurate and that no further testing would be needed to

determine the porosity. 67MPa samples required more testing to determine the porosity, when there were at least three repeatable readings, an average of the curves was taken; see figure 28.

| **Stress** | Undamaged | 34MPa | 67MPa | 101MPa | 135MPa | 110°C | 135°C |
|---|---|---|---|---|---|---|---|
| **Number of Tests** | 4 | 3 | 3 | 9 | 7 | 12 | 4 |

Table 4: Number of Tests Run For Each Stress

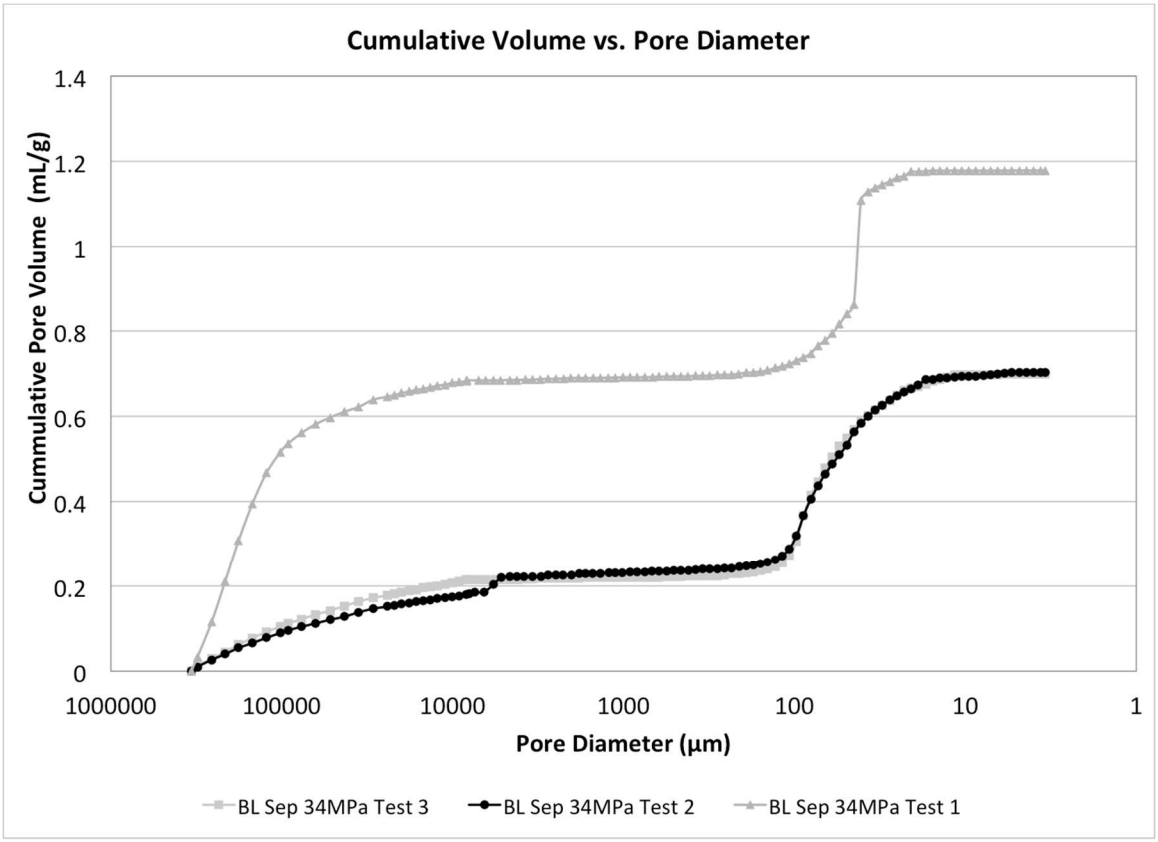


Figure 27: 34MPa Cumulative Volume vs. Pore Diameter

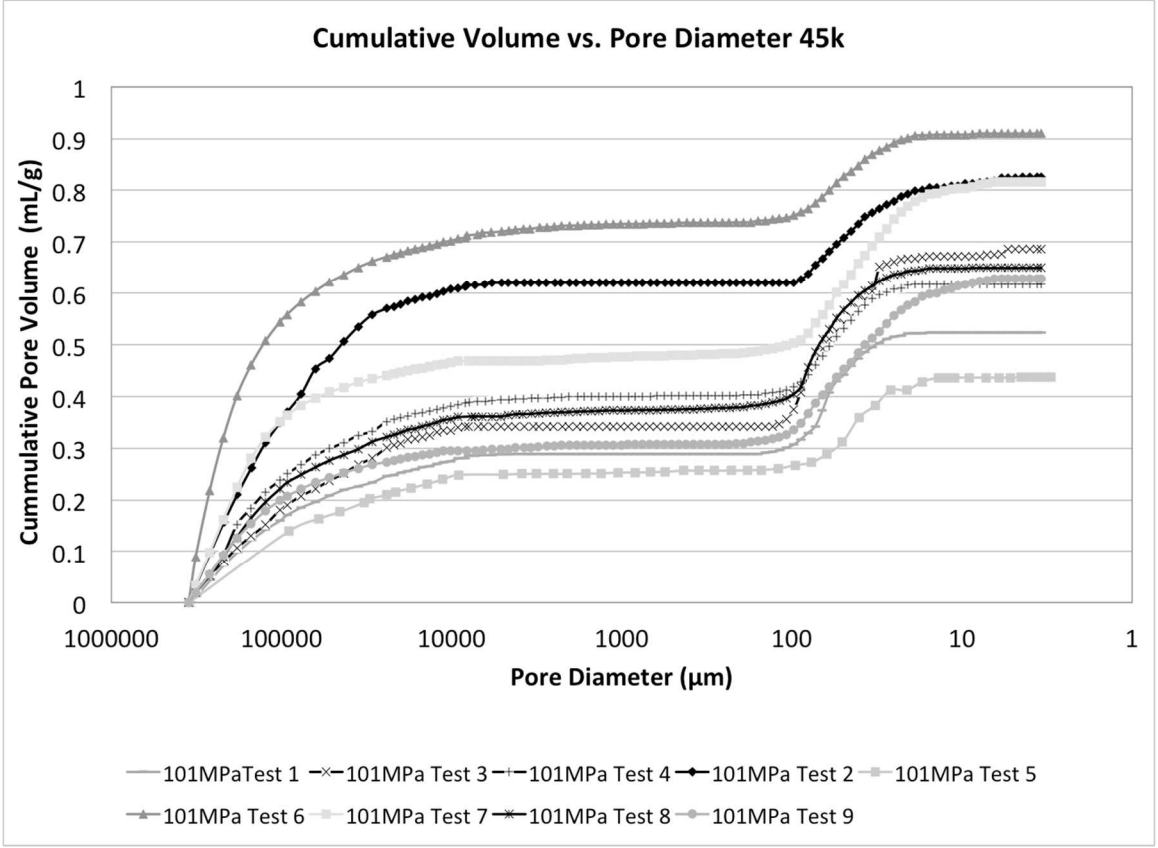


Figure 28: 101MPa Cumulative Volume vs. Pore Diameter

In multiple samples that failed, a dark grey area on the separator formed during the test, as seen in Figure 29. There are a few possible reasons as to why some tests revealed this dark grey substance. The first possible reason is that the sample is going under a process called embrittlement. Embrittlement is a phenomenon when the structural integrity of an object (usually a metal) is changed by making it brittle due to a liquid metal (in this case mercury) [38]. Embrittlement is a form of corrosion and can occur under high pressures, although, embrittlement seems unlikely to influence a plastic separator. The second reason is that the mercury is getting trapped inside of the separator during the test. The third reason

is that the separator is going through a chemical reaction. Other reasons why samples failed include, a rip being in the separator, a contaminant got inside of the penetrometer, incorrect weight measurements, excessive vacuum grease, insufficient torque of penetrometer cap, etc.

Figure 29: Dark Grey Patch on Separator Sample

2.3.3) Mercury Intrusion Results

The Mercury Intrusion study revealed much about the porosity of the battery separators. The porosity of the baseline sample was found to be 41%±1%. This result is consistent with the known porosity given by the separator's manufacturer, Celgard, demonstrating that the Mercury Intrusion tests results are valid. The remaining samples porosities are shown in Table 5. Another result drawn from the Mercury Intrusion tests was the "shifting of the pore sizes" in the separators under a

greater stress as can be seen in Figure 31. When under an initial stress, the larger pores are compressed enough to form smaller pores. Comparing Figure 30 with Figure 31, it can be seen in Figure 30 that the 34MPa and the 67MPa absorb a similar amount of mercury, and their porosity readings are very similar. However in Figure 31, it can be seen that the 34MPa has more of the larger pores than the 67MPa suggesting that between 34MPa and 67MPa, the large pores are just compressing into smaller pores, not affecting the total porosity as much. Until higher stresses are reached, (101MPa, 135MPa, 110°C & 135°C) the porosities decrease and their pore diameters (Figure 31) begin to also decrease suggesting that, that is where the pores are beginning to close, lowering the total porosity.

| Stress | Undamaged | 34MPa | 67MPa | 101MPa | 135MPa | 110°C | 135°C |
|---|---|---|---|---|---|---|---|
| Porosity | 41±1% | 35±1% | 32±1% | 21±3% | 18±2% | 27±1% | 19±5% |

Table 5: Mercury Intrusion Porosities

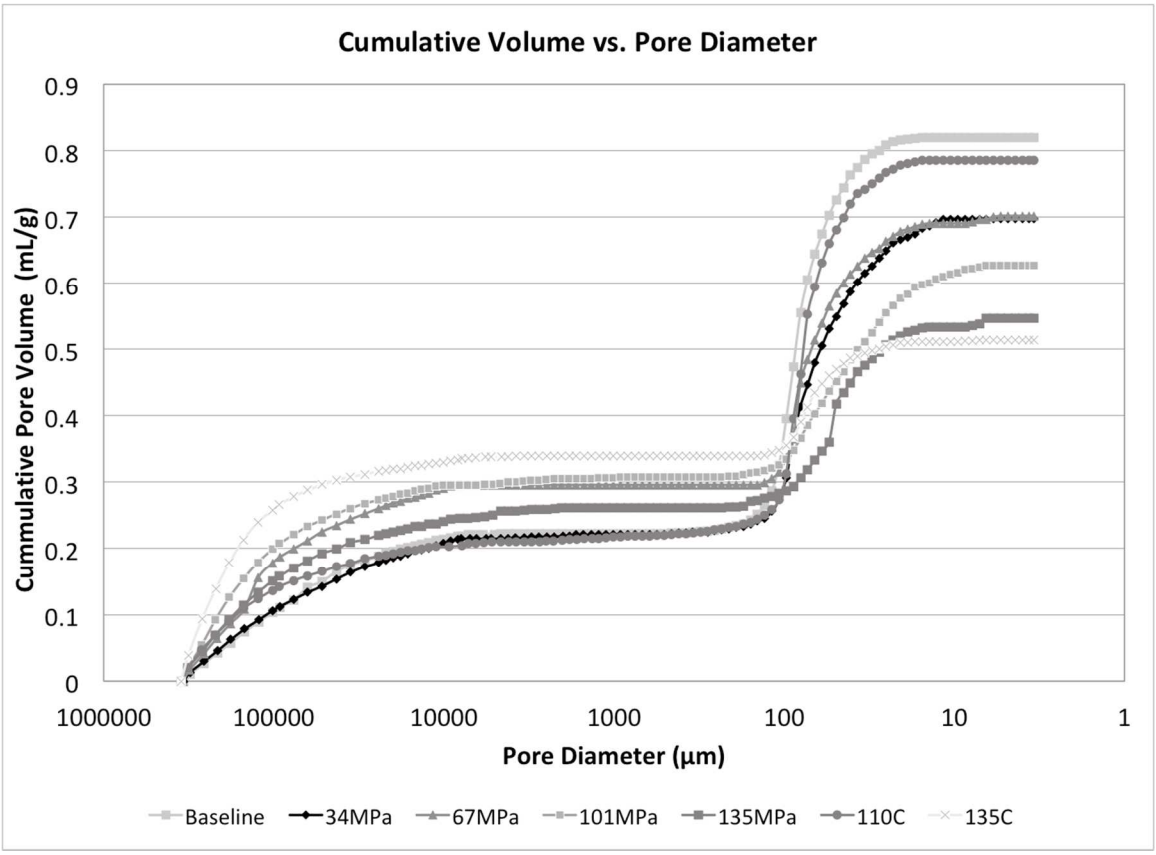


Figure 30: Cumulative Volume vs. Pore Diameter

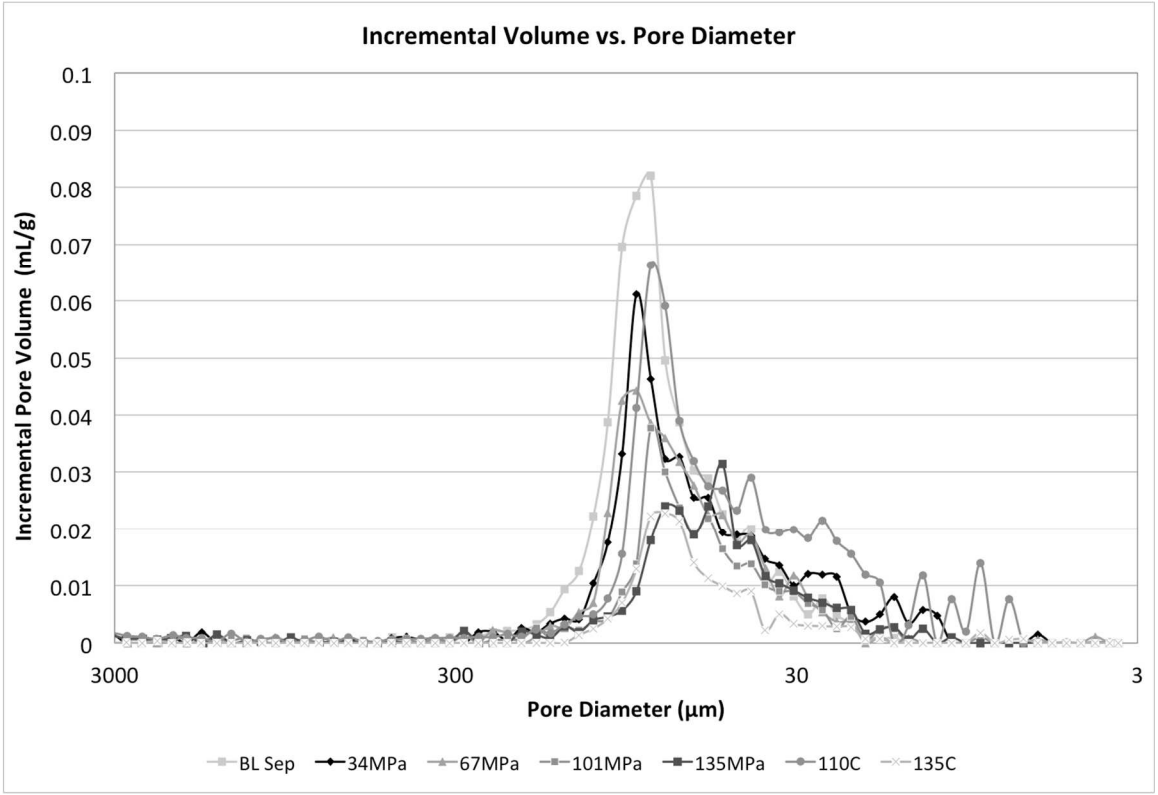


Figure 31: Incremental Volume vs. Pore Diameter

## 2.4) Thermal Shrinkage

Although the porosity of the 110°C separator decreased by approximately 15%, the thickness remained relatively consistent compared to the baseline separator. The pore walls closed despite the separator retaining it's thickness. A thermal shrinkage test was conducted to determine if the PP-PE-PP material was actually expanding during thermal abuse to close the pores or if the material was contracting to close the pores. Thermal shrinkage tests have been conducted before on PP-PE-PP separators such as in [14, 15, 13, 24, 25, 37]. However, these tests have more described the shrinkage percentage % at either the automatic shutdown point (135°C) or the point at which the separator begins to deform (80°C and 90°C). The

purpose of this thermal shrinkage test was to observe the shrinking of the separator in between 80°C to 135°C as well as confirm observations made from these previous tests. A similar equation to Equation 3 was used to determine the thermal shrinkage % in separators by Song et al in a similar experiment [24].

$$\text{Thermal Shrinkage \%} = \frac{A_o - A}{A_o} \times 100 \qquad (3)$$

2.4.1) Setup and Procedure

A hot plate was used to heat the separators uniformly. Each separator sample was cut to 40mm by 40mm squares using an XACTO knife. The hotplate was heated to the desired temperature (starting at 80°C) and the temperature was confirmed using a thermocouple. Before and after heating pictures (Figure 32 A & B) were taken of each sample to measure the difference in area using the ImageJ program. Samples were once again heated for 3 minutes each with a steel plate placed on top of the separator. Starting with 80°C, samples were heated in 10°C increments until 130°C in which the next temperature was 135°C or the automatic shutdown temperature (80°C, 90°C, 100°C, 110°C, 120°C, 130°C and 135°C).

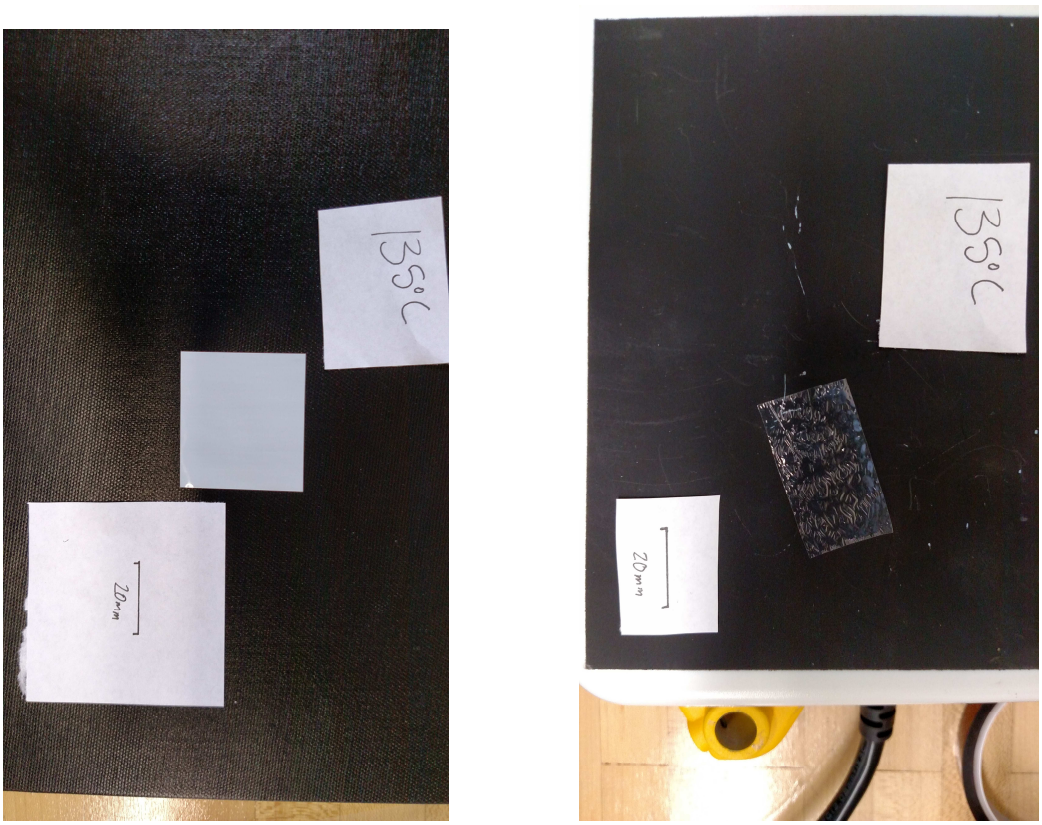


(A) (B)

Figure 32: A & B Before and After Picture of a Sample Heated to 135°C

2.4.2 Thermal Shrinkage Results

As the temperature applied to the separator material increases, the total area decreases. The resulting thermal shrinkage percentages (using Equation 3) can be seen in Table 6. As can be seen in Figure 33, the thermal shrinkage begins to rise between temperatures 110°C and 130°C. The thermal shrinkage demonstrates how the heated samples can have a similar porosity as the crushed samples, even though their thickness does not change the same rate. The pores close by the walls of the pores closing in, this is done by either the separator closing from the sides and/or the separator walls being crushed and pushing outwards. The separators' thermal shrinkage appeared asymmetrical as seen in Figure 32(A & B). At 80°C the separator

should show little signs of shrinkage, and at 90°C, the separator's thermal shrinkage percentage should be under 5% [13]. Since the results of the thermal shrinkage test were consistent with the aforementioned percentages, the test was determined to be an accurate representation of the separator reaction to a thermal stress.

| **Temperature (°C)** | 80 | 90 | 100 | 110 | 120 | 130 | 135 |
|---|---|---|---|---|---|---|---|
| **Shrinkage (%)** | 0.7 | 3.2 | 5.3 | 7.2 | 19.2 | 36.8 | 38.2 |

Table 6: Thermal Shrinkage Results

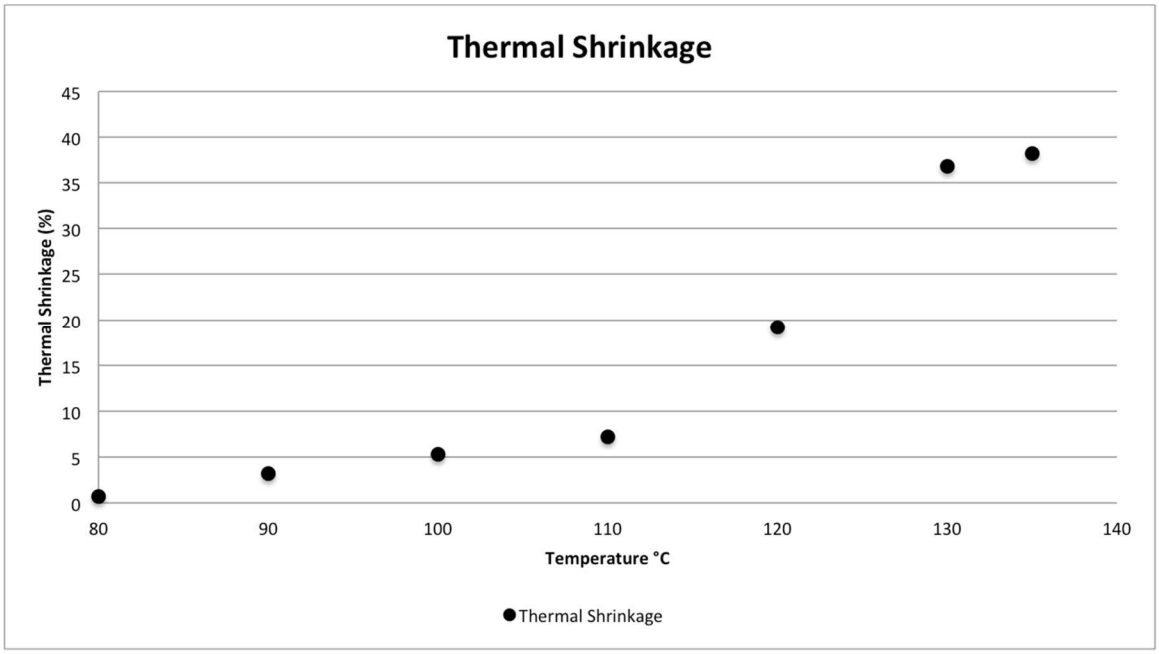


Figure 33: Thermal Shrinkage Graph

## 2.5) Discussion of Results

When comparing the results between the SEM and the Mercury Intrusion, it can be determined that the automatic shutoff appears to be working properly. The SEM and the Mercury Intrusion showed a change in the pore size and shape as well as the porosity of the separator. When a stress is induced upon Celgard 2325, the separator thickness decreases as seen in the results from 2.2.1, the pores close and the porosity drops. However, when the separator is subject to a higher thermal stress, the pores close at a higher rate than the separator thins as seen when comparing results from 2.2.1 and 2.2.3. The pores are still able to close due to the separator's face area shrinking, it seems the porosity of the separator is related to the volume of the separator, not just the thickness. Pore closing limits the ions transfer, effectively shutting off the battery. Interestingly, it seems that there is a period between a fully functioning battery cell and the automatic shutoff of the battery cell as the porosity does not drop significantly until a higher stress is present. Future work should be conducted for comparison between a fully functioning cell and a complete shutoff of the cell to better understand what the cells capabilities are in the cell after damage.

# CHAPTER 3. Effects of Stress on Separator on Battery Capacity

Much of what has been studied about battery separator is either the performance of undamaged separators, battery cell shutdown, or internal shorts thru the separator. An opportunity exists to study the performance of damaged separators in between the automatic shutdown and the undamaged phases. This chapter investigates the battery cell's performance with damaged separators.

## 3.1 Coin Cell Testing with Damaged Separators

To observe the effect a damaged separator plays on a battery cell, custom Lithium Ion cells with damaged separators were manufactured and cycled to monitor their capabilities. Based on the relatively small scale and low capacity, it was determined that the best and safest way of testing damaged separators was to test them inside of coin cells. The benefit of using coin cells is that they can be easily controlled and cycled using the Arbin as well as being relatively easy to build. A coin cell building schematic can be seen in Figure 34.

First, a stress was applied to the separator layers using the same method done for the porosity samples. Compressing the separator area using the Instron machine at stress increments: 33.71MPa, 67.42MPa, 101.13MPa and 134.84MPa. Coin cells using separators subject to thermal stresses of 110°C and 135°C were also tested. This time, instead of a 19mm x 81mm compressed area, a 25.4mm by 25.4mm area was employed. A 19mm diameter circle was removed from the compressed area of the separator as a component for manufacturing the coin cell.

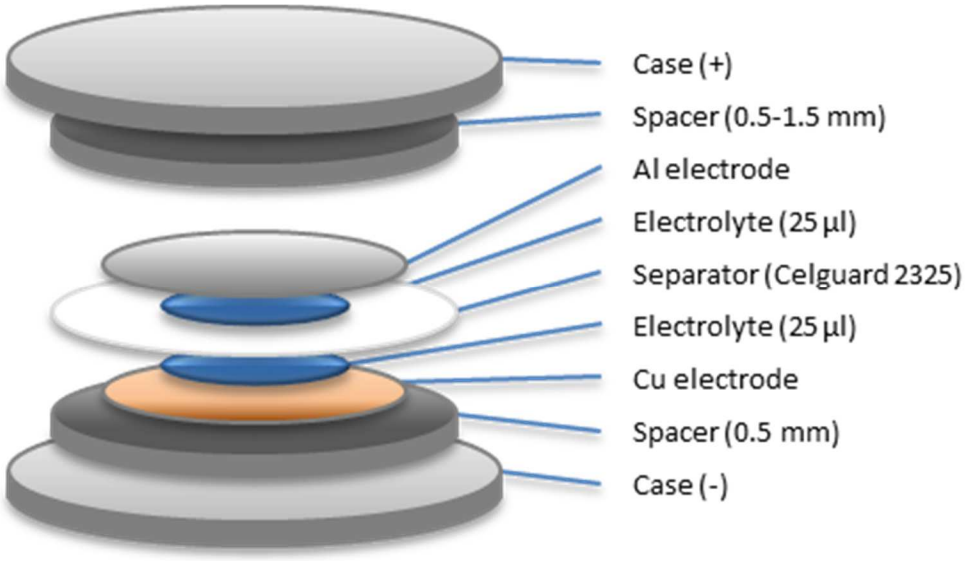


Figure 34: Diagram of Coin Cell using Celgard 2325 Separator

3.1.1) Experimental Approach

Three coin cells of each stress level were created as well as three coin cells with an undamaged, baseline separator. This was done to assure accurate results. The Arbin cycles batteries by first applying a positive current (+) to charge the battery, then a negative current (-) to discharge the battery. This charge then discharge is the equivalent of one cycle. Each coin cell was observed over its first 20 cycles. The first 3 cycles were the formation of the coin cells, while the next 17 cycles were cycles to simulate use a cell would see in application. Each 1.6 mAh coin cell was cycled using the same currents during the same cycles to assure an accurate comparison as seen in Table 7. It should also be some of the coin cells did not complete their full cycling procedure seen in Table 8.

| Cycle Number | Charge Current (mA) | Discharge Current (mA) |
|---|---|---|
| 1 & 2 | 0.298 | -0.298 |
| 3-19 | 1.470 | -1.510 |
| 20 | 1.47 | -7.470 |

Table 7: Coin Cell Cycling Setup

| Stress Level | # of Coin Cells Cycled | # Completed 20 cycles |
|---|---|---|
| Baseline | 3 | 3 |
| 34MPa | 3 | 3 |
| 67MPa | 3 | 3 |
| 101MPa | 3 | 1 |
| 135MPa | 3 | 1 |
| 110°C | 3 | 1 |
| 135°C | 3 | 1 |

Table 8: Coin Cell Testing Overview

3.1.2) Cycling Results

Discharge capacity was chosen as a representation of the overall capability of the coin cells. Experiments conducted on different Li-Ion coin cells at different charge and discharge rates completed by Li et al, used discharge capacity to determine the abilities of these different Lithium Ion cells [39]. Figure 35 shows the

discharge capacities of damaged cells. This method was chosen because not all of the cells made it through the 20 cycles. Cells were chosen that continued to register a discharge capacity through their $20^{th}$ cycle. It should be noted that although each cell chosen retained a measurable capacity after 20 cycles, the cycle lives of some cells are below 20 cycles. According to Richard Perez in the "Complete Battery Book", cycle life is generally considered as the amount of cycles before the battery capacity drops bellows 80% of its original capacity [12]. Using Equation 4, to determine charge efficiency, a of the Discharge Capacity (DC) compared to the Original Discharge Capacity ($DC_o$), the 135MPa and 135°C samples had cycle lives of 3 and 2 cycles respectively.

$$\text{Capacity \%} = \frac{DC}{DC_o} \times 100 \qquad (4)$$

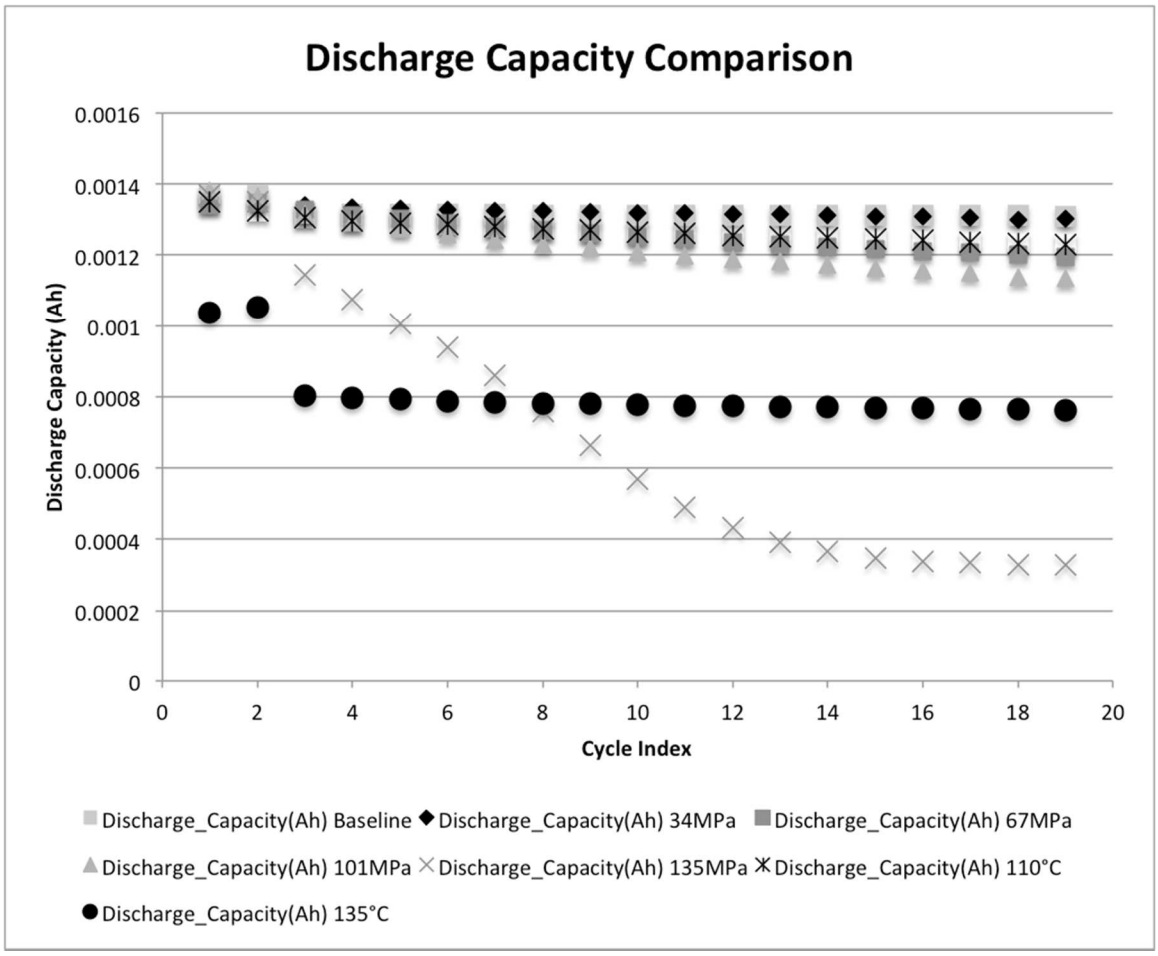


Figure 35: Discharge Capacity Comparison

## 3.2) Experimental Results and Discussion

Using the data obtained from Chapter 2, comparison between the discharge capacity with the separator porosity and the discharge capacity versus separator thickness was made possible. Looking at Figure 35, one can immediately see that the 135MPa compression as well as the 135°C heating have much lower discharge capacities. This can be expected since their porosities (18%±2 and 19%±5% respectively) are lower than the baseline undamaged separator (~40%). However, the data shows unexpected phenomena that instead of operating at a certain

capacity and maintaining that until failure, it seems that in some cases, the cell loses discharge capacity with each cycle until ultimately failing. The 135MPa sample demonstrates this phenomenon, showing the steep negative trend in discharge capacity to a point in which the battery capacity is below functional levels.

To observe the discharge capacity of the other samples (baseline, 34MPa, 67MPa, 101MPa, and 110°C), 135MPa and 135°C were ignored in Figure 36 since their cycle lives' were less than 20 cycles. Observations can be made when investigating the capacity of lower stress levels. First, the baseline and the 34MPa have very similar discharge capacities through their first 20 cycles. Second, all cells start at a very similar discharge capacity (around 0.00135 Ah) during their first cycle. Although starting at similar discharge capacities, the damaged cells have considerably different discharge capacities at the end of 20 cycles. The third observation made from Figure 36 is that although the 110°C separator has a lower porosity than the 67MPa separator, the 110°C separator that cycled all 20 cycles had a high discharge capacity at the end of 20 cycles than the 67MPa. Each of these observations are observed in greater depth in the following sections.

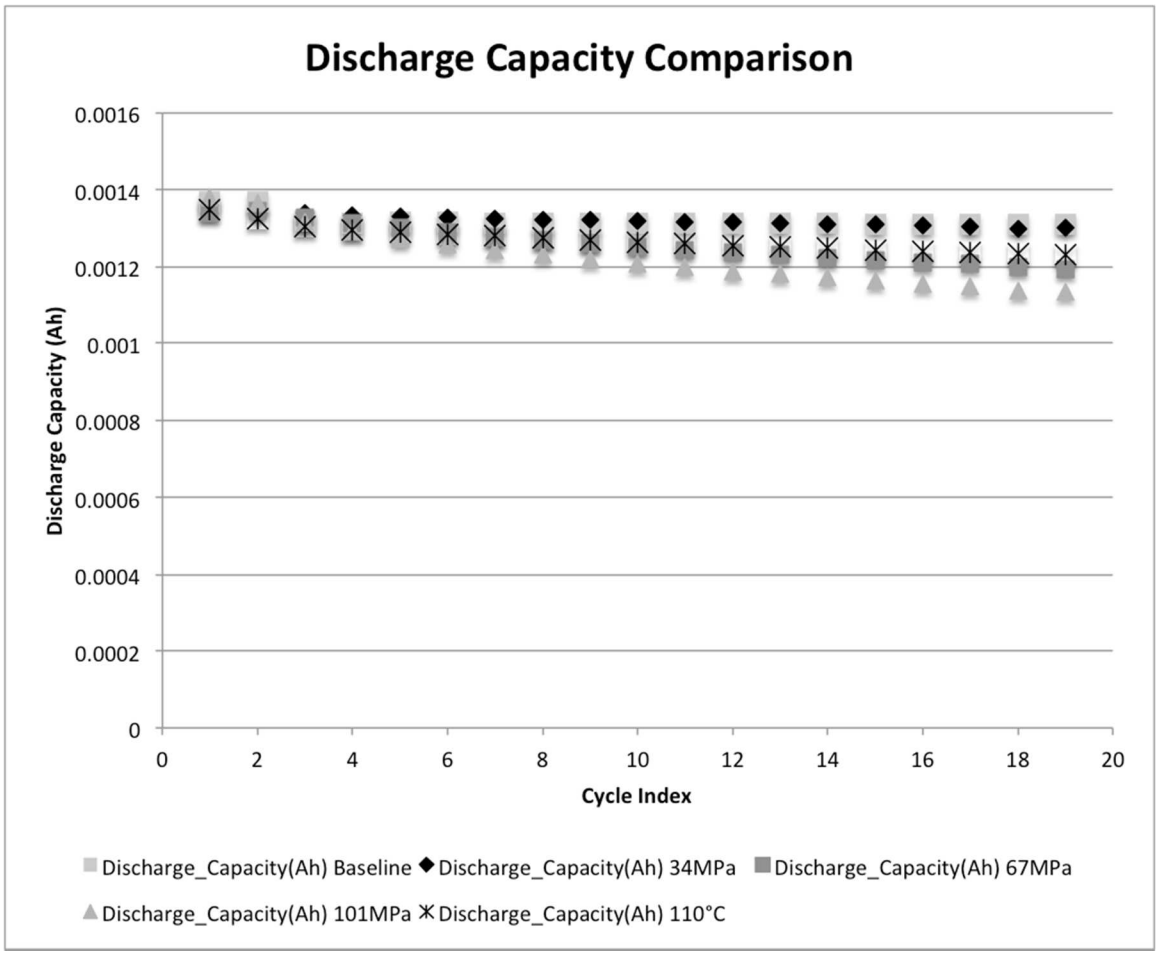


Figure 36: Discharge Capacity Comparison Excluding 135MPa and 135°C

3.2.1) Baseline vs 34MPa

The baseline or undamaged separator had a very similar discharge capacity throughout the first 20 cycles, as can be seen in Figure 35. However, investigated at a finer scale, such as in Figure 37, the discharge capacity curves are not the same. The baseline curve starts at 0.00137Ah for 2 cycles before quickly dropping to around 0.00131Ah where it levels out. The 34MPa on the other hand, starts at 0.00136Ah and begins a rather constant descent to 0.0013Ah by its 20$^{th}$ cycle. This seems to demonstrate what can be seen in the other damaged cells but on a much

smaller scale. The 34MPa curve looks similar to the 135MPa curve from Figure 35, just on a smaller scale. It seems, like the 135MPa, the 34MPa's discharge capacity will eventually fall to the point of being ineffective. However, it should be noted that the cycle life of the 34MPa will be relatively high.

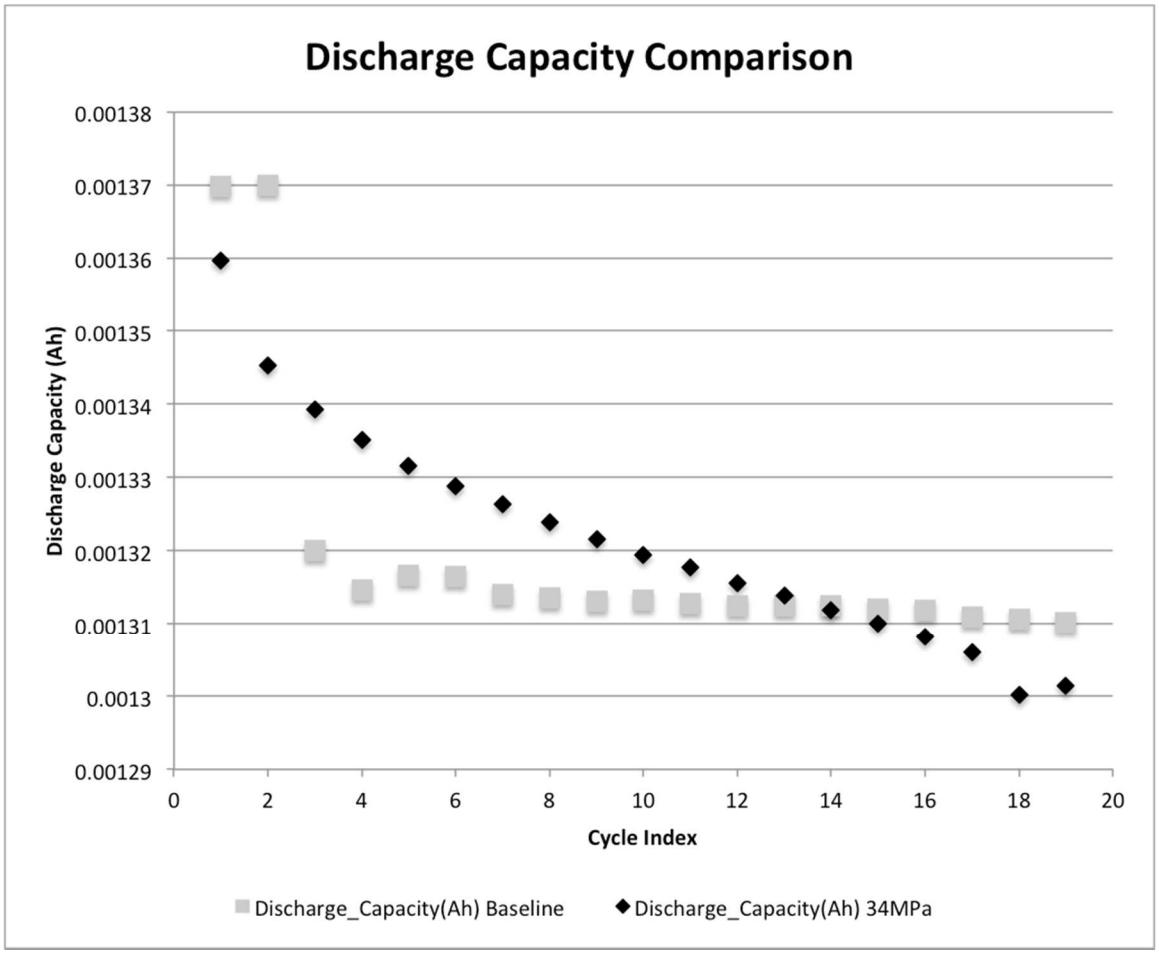


Figure 37: Discharge Capacity Comparison Between Baseline and 34MPa

3.2.2) 1st vs. 20th Cycle Discharge Capacities

Another observation that can be made from Figure 35 is the difference in discharge capacities from cycle 1 to cycle 20. As discussed earlier, after the 20th cycle, all of the damaged separator cells have a lower discharge capacity than the baseline. Perhaps the more interesting observation is during cycle 1, in which most of the cells (excluding 135°C) have a very similar discharge capacity. Each damaged separator has a lower porosity than the baseline separator. This explains why the cells with the damaged separator have lower discharge capacities in cycle 20 since the ions require the porous openings to transfer from electrodes.

Figure 31 demonstrates that when separators are subject to a stress, the first pores to be transformed are the larger pores which seem to be compressed into smaller pores. The reduction of large pores into small pores is the leading cause of the loss of discharge capacity. Perhaps over the course of cycling, ions are trapped in the smaller pores. Once lithium ions are trapped, they close the pores, leaving fewer channels for the ions to pass through. The reason the discharge capacities are similar at the first cycle would be because the number of unclogged pores are the same, even if the size of the pores are different. During the first cycle, none of the pores would be clogged while during the 20th cycle, many of the smaller pores would be closed up, this would explain why capacity trend of damaged separators' exhibit a steep decline.

Another potential reason why the damaged separators are similar to the baseline during cycle 1 but different during cycle 20 could be that geometry of the ion channels exist through the separator but are closed. Looking back at Figure 23

from chapter 2, various pathways exist in the center layer in which ions can travel between electrodes. Perhaps some of these pathways become damaged and even close.

These hypotheses for understanding the difference in discharge capacity from the first cycle and 20$^{th}$ cycle will require more research to determine the validity. It seems unlikely that the difference is based on chemistry because the surface area on the anode and cathode are uniform in all cells and the anode and cathode are undamaged in all cells. Also, the same amount of electrolyte is in all cells. With all of the variables being the same, the focus must remain on the separator.

### 3.2.3) 67MPa vs. 110°C

The final anomaly as observed from Figure 35 is the difference in discharge capacity between the 67MPa and 110°C cells. The 110°C separator has a lower porosity than the 67MPa separator (27%±1% and 32%±1% respectively) as seen in Table 5. However, in Figure 38, the 110°C cell had a higher discharge capacity at the end of the 20$^{th}$ cycle. For the rest of the cells, the lower the porosity, the lower the discharge capacity at the 20$^{th}$ cycle. This could be due to the 110°C separator having more "large pores" than the 67MPa separator, as seen in Figure 31 from Chapter 2. The "large pore theory" is consistent with first theory from 3.2.3. However, looking at the SEM images from Chapter 2 (Figure 15 through 21), it can be seen that the two stresses deform the pores differently. The 67MPa compressive stress compresses the size the pores at a different orientation, forming long narrow

openings. While the 110°C stress deforms the pores from every angle making the pores slightly smaller versions of their earlier selves. If in fact the pores are being deformed in this manner throughout the separator, it may just be making the pathways narrower rather than closing them off completely.

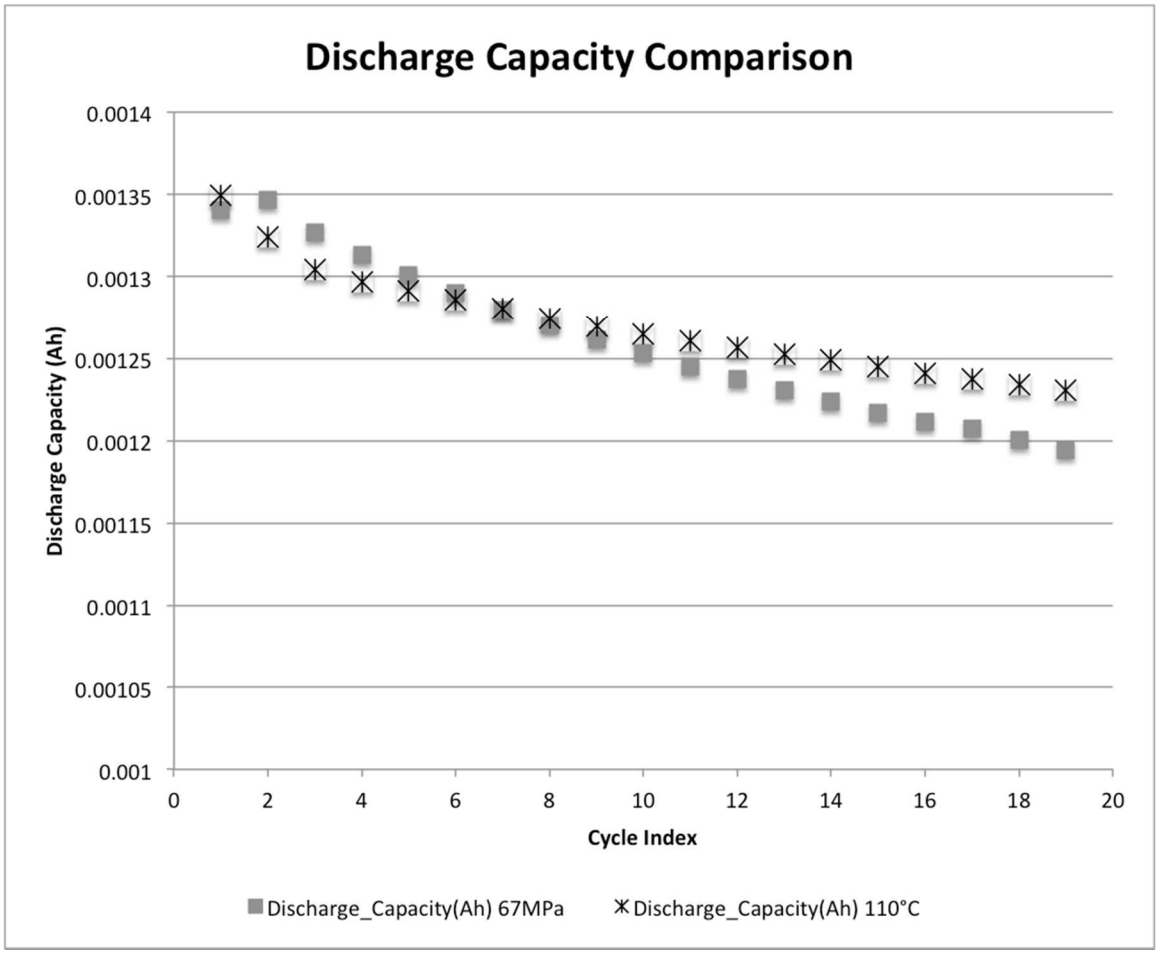


Figure 38: 67MPa vs. 110°C Discharge Capacities

# CHAPTER 4. Effect of Porosity on Thermal Output of Battery

Once the internal effects on a cell had been observed after subjecting a separator to a stress, it only made sense to observe an external effect on the cell. In order to observe the thermal impact of the separator on a battery cell, it was decided to use pouch cells as to hopefully generate more heat than that of a coin cell. Pouch cells have been used in the past to observe heat generation mostly in catastrophic failure type analysis such as conducted by Finegan et al in which pouch cells were subject to high heat until thermal runaway was induced [40]. Many of the catastrophic failure analysis has been observing nail test penetrations, as discussed earlier in chapter one, in which a nail is thrust through the outer layer of the pouch cell exposing the innards of the cell to oxygen [31]. As opposed to damaging parts of the cell after the cell is complete, like in the earlier tests [33, 32], separators were damaged before production of the pouch cell. This gave the advantage of isolating the effects of the damaged separator rather than damaging the cell as a whole like in the nail penetration tests.

## 4.1) Pouch Cell Testing with Damaged Separators

Investigation of battery thermal response was conducted on pouch cells much larger than the coin cells in the discharge capacity study. The research extends into the thermal domain in order to determine a sufficient number of layers to generate heat while remaining safe to operate at C-Rates above 1C. Beginning with a single layer pouch cell, it was determined that the capacity of the cell was not enough to monitor temperature fluctuating using the accuracy of the thermal

camera available. From investigation of a study used by Sahraei et al in which a 3.2 Ah cell was used to create an accurate simulation of a damaged Lithium Ion cell, it was determined that a pouch cell of a similar capacity needed to be employed to assure large enough temperature change to register with a thermal camera [41]. Originally, a thermal camera was chosen to observe the temperature changes of the cell with the hopes of visually monitoring of the thermal propagation in the cell as seen in Figure 39. A study conducted by Kim et al, used a thermal camera to measure the temperature of a pouch cell during charge, which demonstrated that a thermal camera would be able to collect the data needed [42]. Equation 5 was used to determine the amount of layers needed for the pouch cell compare to the one used by Sahraei et al, since the area of the cathode and the desired capacity was known. For safety purposes and to assure accurately stacked layers, 30 layers was determined to be the maximum amount of layered pouch cell that could be constructed. Each Cathode had an active area of $92.71 cm^2$. With 29 cathodes in a 30 layer pouch cell (all but one layer is coated on either side), the pouch cell used in the following experiment had a capacity of 2500mAh or 2.5Ah.

$$\text{Battery Capacity} \approx \text{Area of Cathode}(cm^2) \text{ x } 0.93\frac{mAh}{cm^2} \text{ x (\# of Layers)} \qquad (5)$$

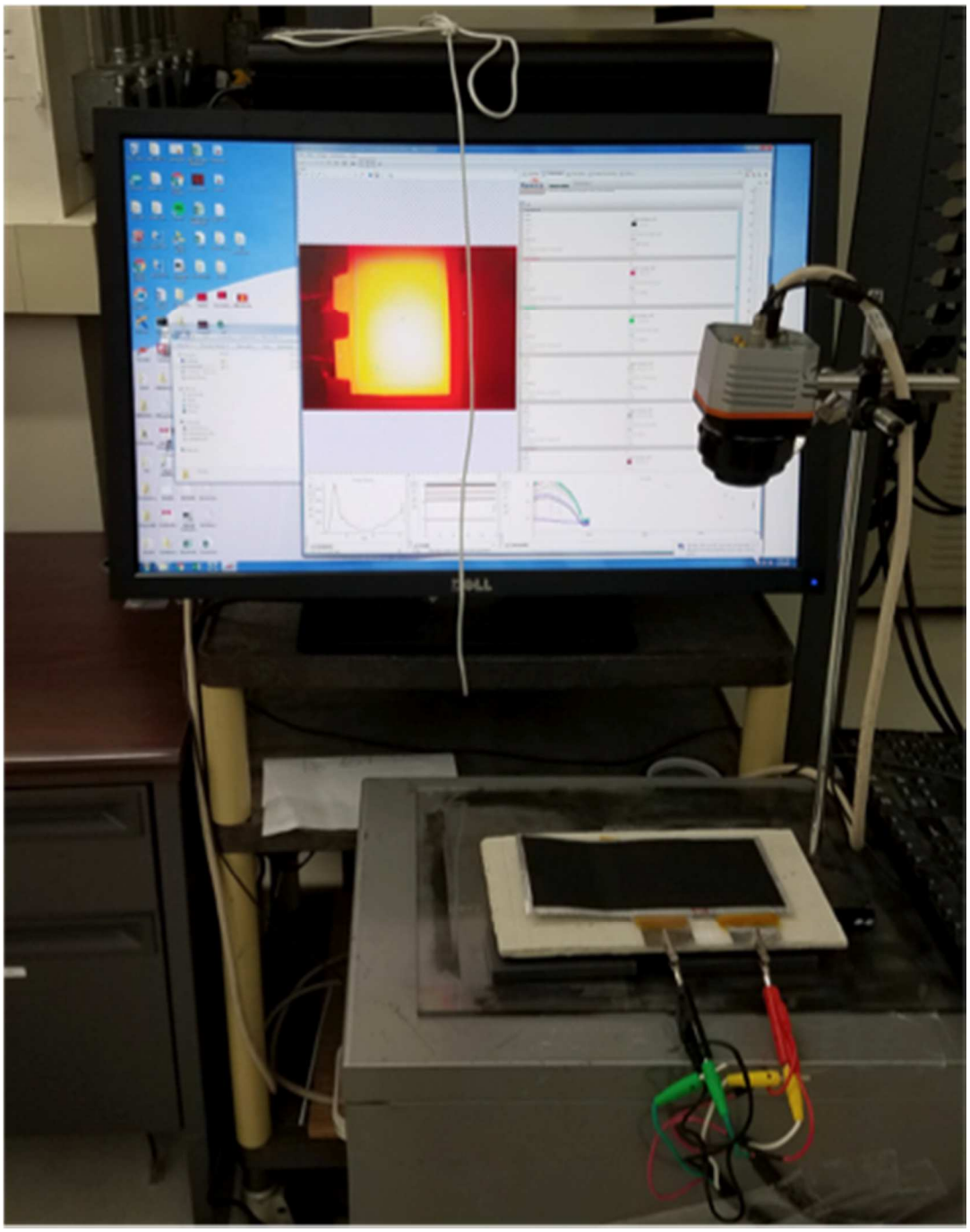

Figure 39: Thermal Cameral Setup

#### 4.1.1) Experimental Approach

The cycling of the pouch cell for the thermal data was very similar to the cycling of the coin cell data with the exception of obtaining thermal data. Thermally abused separators were not observed in pouch cells either due to the fear of an internal short around the edges of the separator caused thermal shrinkage. Once again, the Arbin was employed and the construction of the pouch cell was a similar process to that of a coin cell.

##### 4.1.1.1) Pouch Cell Construction

As stated earlier in section 4.1, it was determined that a 30 layer pouch cell was the best option to observe large temperature changes, while also being relatively safe. Much like the coin cell, the pouch cell consists of an anode, separator and a cathode stacked on top of each other. The anode was copper coated with graphite, while the cathode was aluminum 92% active material (NMC111). The anode and cathode were cut to the sizes specified and stack on top of each other as seen in Figure 40. Each anode and cathode were double sided except the top and bottom layers. This called for 15 anodes cut, 15 cathodes cut and 30 total separators, creating a 30 layer pouch cell. It should be noted that each separator was compressed with the same stress levels as the coin cell experiments. The stress remained constant from the coin cell compression, however, a different sized steel plate was used to compress a greater area at a time (40mm by 45mm). Once all of the layers were stacked accurately on top of each other inside of the pouch cell, electrolyte was poured into the cell, the pouch cell was then sealed and the tabs

sticking out of the pouch cell as seen in Figure 40 were soldered together. Figure 39 shows the constructed and sealed pouch cell. The pouch cell was then monitored to observe any leaks and the top of the cell was painted black so the thermal camera could read temperature changes better. Upon completing these steps, the pouch cell was ready to be cycled.

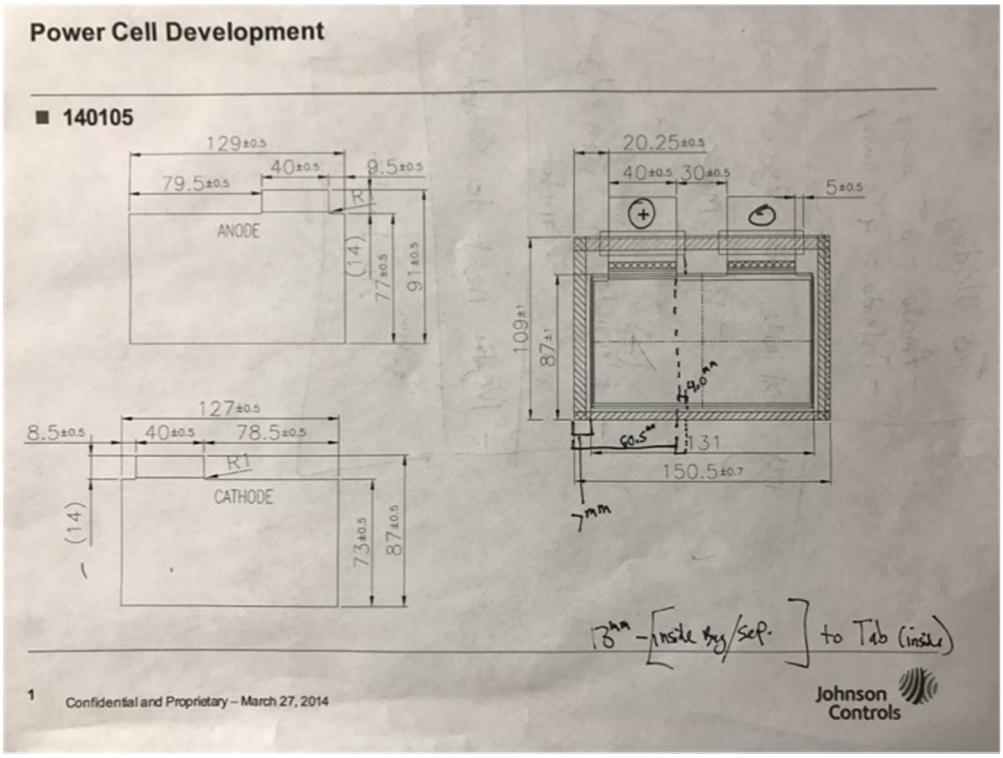


Figure 40: Template for Pouch Cell Construction

4.1.1.2) Pouch Cell Cycling

Much like the coin cells, the 2.5Ah pouch cells were cycled using the Arbin. During formation, the cells were charged at a 1C rate (C-rate is calculated using Equation 6) or 2.5Amps (A) until the Voltage was raised to 4.1Volts (V), then discharged at 1C until the cell was down to 2.7V. During cycling, the cells were charged and discharged at a 3C rate between 4.1 and 2.1V. It should be noted that

the in between the charge and discharge of the cells, there was a hold period in which the Voltage is held at 4.1V until the amperage falls to a designated Amps (different between the formation and cycling of the cell). Each cell was cycled 19 times to be consistent with the coin cell data (disregarding the 20$^{th}$ cycle from the coin cells), the breakdown of the formation and cycling can be seen in Table 9. It should be noted that after discharge, the cell was rested and then charged again.

$$\text{C-Rate} = \frac{Amps}{Capacity} \quad (6)$$

| | **Charge Current** | **Charge To** | **Hold Voltage Until** | **Discharge Current** | **Discharge To** |
|---|---|---|---|---|---|
| **Formation** | 2.5A | 4.1V | 0.125A | -2.5A | 2.7V |
| **Cycling** | 7.5A | 4.1V | 2.0A | -7.5A | 2.1V |

Table 9: Pouch Cell Formation and Cycling

4.1.2) Thermal Results

The peak temperatures of the baseline cell during the discharge remained constant between cycles. Therefore, the peak temperatures over the course of all of the cycles were observed as seen in Table 10. Observing Table 10, the greater the stress on the separator, the higher the peak temperature. The higher peak temperature is correlated with lower porosities of the separators. It should be noted that the 101MPa and 135MPa in Table 10 are projected values, at the time of this experiment safety concerns prevented the manufacturing of these cells. With a

damaged pouch cell of that magnitude, thermal runaway could be extremely dangerous.

| **Cell** | Baseline | 34MPa | 67MPa | 101MPa | 135MPa |
|---|---|---|---|---|---|
| **Temperature** | 26.8°C | 28.7°C | 31.7°C | 36.0°C (Projected) | 42.2°C (Projected) |

Table 10: Peak Temperatures of Pouch Cells with Stressed Separators

# CHAPTER 5. Warm Separator Subject to Compressive Stress

After analyzing separators that had been subject to either a compressive stress or a thermal stress, a combination of the two stresses caused an amplified effect. Tests were run to analyze the effect of a combination of thermal and compressive stresses to observe the porosity and the thickness of the separator.

## 5.1) Separator Subject to Heat and Compression

In order to observe the effect of a combination of heat and compression have on a separator, similar experiments that were used in earlier sections were once again used for the combination samples. Mercury intrusion could once again be used to determine porosity and the 3-D microscope with ImageJ could be used to determine thickness. Knowing the effects of thickness and porosity on a battery cell would aid in understanding of the "combination" stress.

### 5.1.1) Experimental Approach

As discussed earlier, 80°C is the highest temperature a Celgard 2325 separator can be subject to before it begins its deformation. Observations from the thermal shrinkage experiment in Chapter 2 are consistent with this claim. Once again, an Instron was used to compress the separator samples to the desired stress. To heat the separators to 80°C as they were being crushed, the steel cylinders used to crush the separators were heated in an oven to 80°C. The cylinders were heated to 80°C for 24 hours before the crush and the cylinders were determined to be of adequate size so that they could maintain a similar temperature for the duration of a

crush. Each separator sample was crushed at 33.71MPa in order to be comparable to earlier tests. Once samples were ready, mercury intrusion or 3-D Microscopy were conducted on the samples to determine porosity and thickness respectively as had been conducted in Chapter 2.

### 5.1.2) Results

A separator crushed at 80°C showed differences when compared to a separator crushed at room temperature (~21°C). The magnitude of the difference between the two crush temperatures, that were heated to 80°C while being crushed had a porosity of 11±1% while separators being crushed with the same stress (34MPa) at room temperature had a porosity of 35±1%. As seen in Figure 41, barely any mercury could be pushed into the pores of the 80°C crushed sample compared to the room temperature sample during their respective mercury intrusion tests. The lack of mercury being pushed into the combination sample compared to the 34MPa sample in Figure 41 offers a visual of the difference in porosity. Figure 42 demonstrates the distribution of pores sizes in the two samples. In Figure 42 the peak of the pore sizes completely shifts between the different stresses and also shows just how many pores have closed completely.

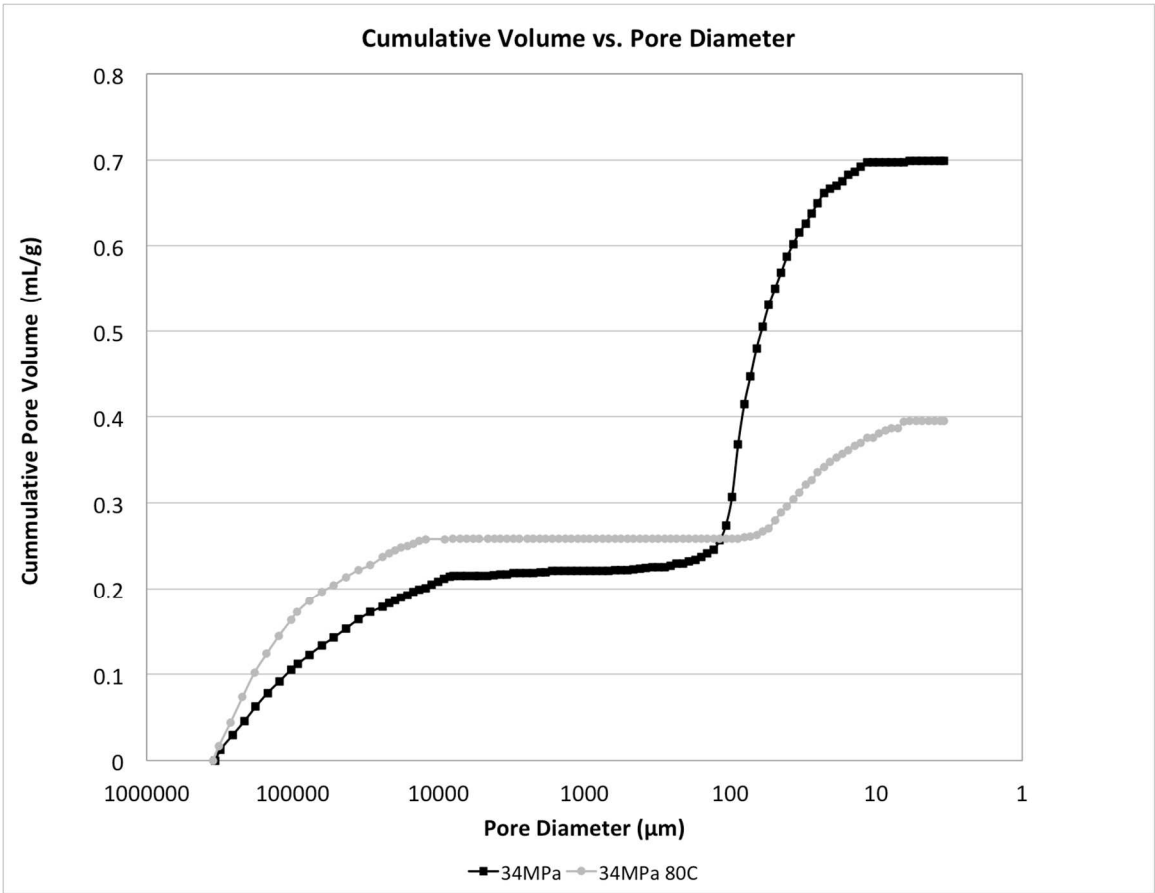


Figure 41: Hg Intrusion Compressed vs. Heated and Compressed

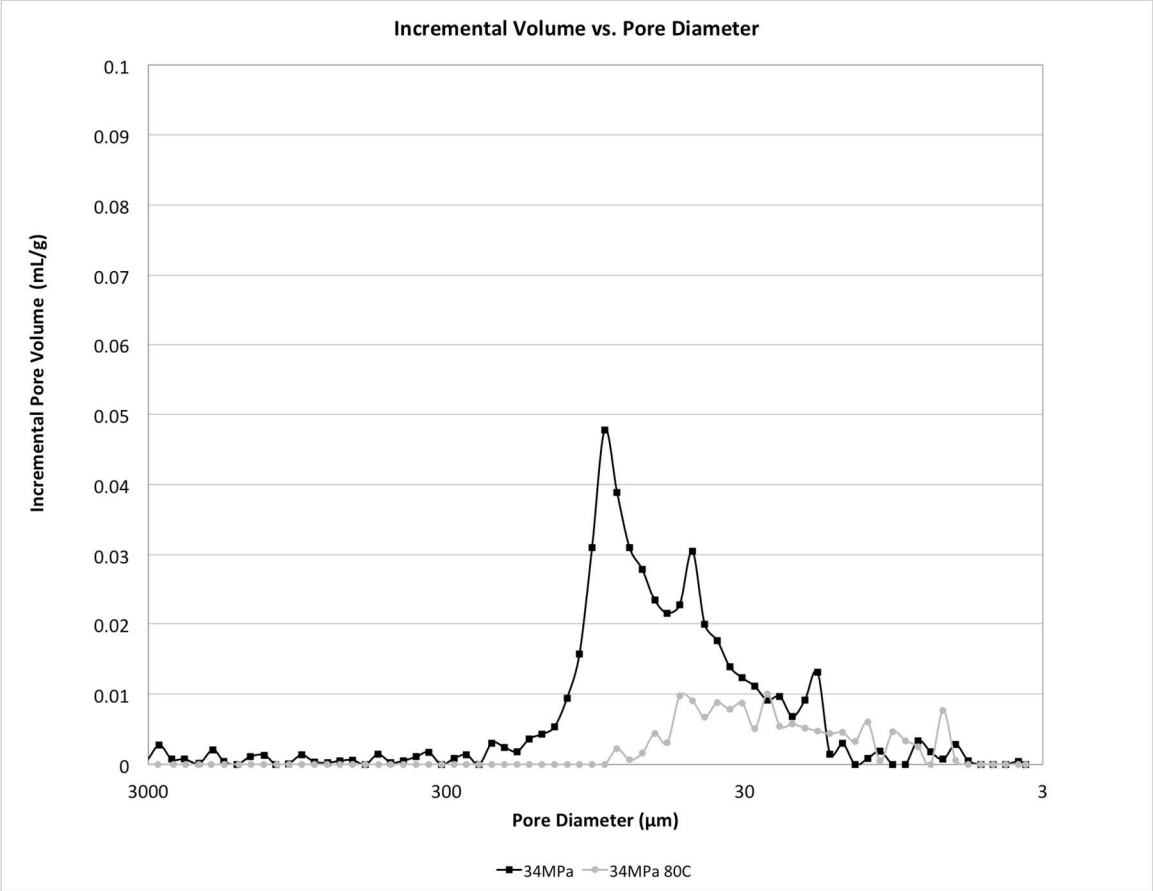


Figure 42: Incremental Pore Volume Compressed vs. Heated and Compressed

5.1.3) Discussion

The combination of a compressive stress with warming the separator caused the compression effects to be amplified. Previous testing concluded that thermal deformation doesn't take effect until after 80°C [36] and thermal shrinkage tests in Chapter 2 confirmed this assertion. However, thermal stress ≤ 80°C weakens the separator enough to be compressed at a higher rate. This finding was important in understanding the functionality of a battery inside of an instrument that may be subject to a compressional stress while cycling, such as a car or cell phone. Thermal testing done in Chapter 4 confirmed that a cell's temperature increases when

cycling. For example, if a car were to get into a crash after the battery is warmed from cycling or some other defect, then the separator would reach it's automatic shutdown point faster than if the car battery was at a lower temperature. It also suggests that lithium-ion cells used in warmer environments would reach its automatic shutdown sooner than a cell in a colder environment.

# CHAPTER 6. Conclusion

## 6.1) Summary

In summary, the purpose of the project was to observe the battery separator Celgard 2325 in between fully functioning and automatic shutdown. Much was already known about the performance of the separator as an undamaged sample and much was known about the lack of performance after it had hit its shutdown point. To observe this unstudied range of stress, the point between when the separator was undamaged and failure needed to be established. The undamaged and failure points were established by results from previous tests by multiple outlets, and confirmed with testing during the course of this research. The unstudied range was then observed in what could be broken down into two categories. The first category being the observations of the effect of a stress on the separator itself; Mercury Intrusion, SEM imagining, 3-D microscopy, and ImageJ were all used to observe the effects on the separator. The second category was the effects of a stressed separator on a live battery cell; Arbin data on coin/pouch cells and thermal data on pouch cells were used to observe this effect.

## 6.2) Conclusions

An understanding of what happens when a separator is damaged is presented from the observations of this project. Much of what was demonstrated by these experiments was indicated without enough investigation or confirmation. However, any result, expected or unexpected is helpful in truly understanding the effect that the separator has on a battery cell. For example, it could be assumed that

a warmed separator subject to a compression stress would deform more than a separator subject to a stress at room temperature, but until the theory was tested and the results confirmed it, there was no way to know it as a fact. However, there were some results from this project that showed results that were unexpected. For instance, it seems that damaged separators' capacity drops over the amount of cycles it has until it ultimately fails, compared to running normally until an abrupt failure which was assumed to be true before the results from Chapter 3 were known. The research conducted in this project showed a correlation between a battery separator subject to a stress and the porosity of the separator. Porosity effected the capacity of the battery cell as well as the thermal output of the cell. The lower the porosity of the separator, the lower the cycle life of the cell and the higher the temperature peaks during cycling of the cell. This project demonstrated that the separator is not just a safety measure, but is also an integral part in the batteries' effectiveness.

## 6.3) Future Work

Although much of this project observed the separator on a microscopic level, an even smaller scale would be beneficial. One area that could use more observation and testing is what exactly happens inside of damaged separator when the ions are passing back and forth between charge and discharge. Data from the Arbin indicates that the ions are getting stuck in a damaged separator as the cell is cycled. However, it was difficult with the equipment available study this theory.

Further thermal testing with damaged separators would also be another pursuit. Testing would have to take place in a controlled environment in which thermal runaway would be manageable such as an environmental chamber that monitors the temperature of the cell with the ability to control the current to the cell if the temperature were to increase to a dangerous level.

The findings in this study will aide in producing the parameters for computer simulations of Lithium Ion batteries during stress. Simulations give companies who make batteries a relatively affordable and safe alternative to live testing. These simulations could be instrumental in making Lithium Ion batteries more safe.

## References


[1] Jeff Tollefson. (2015). Global-warming limit of 2 °C hangs in the balance. *Nature, 520*(7545), 14-15

[2] Lu, Han, Li, Hua, & Ouyang. (2013). A review on the key issues for lithium-ion battery management in electric vehicles. *Journal of Power Sources, 226*, 272-288.

[3] Doughty, D., & Roth, E. (2012). A General Discussion of Li Ion Battery Safety. *Interface Magazine, 21*(2), 37-44.

[4] Mankowski, Kanevsky, Bakirtzian, & Cugno. (2016). Cellular phone collateral damage: A review of burns associated with lithium battery powered mobile devices. *Burns, 42*(4), E61-E64.

[5] Hollister, S. (2016, October 10). Here's Why Samsung Note 7 Phones Are Catching Fire. Cnet, 1-11.

[6] Herron, D. (2015, November 13). Chevy Volt Battery Pack Fire in 2011. The Long Tail Pipe, 1-33.

[7] Woollastan, V. (2013, October 3). New Blow For Tesla: Fire In 'World's Safest Electric Car' Began in Vehicle's Battery. Daily Mail. Retrieved 2017.

[8] Trattnig, G., & Leitgeb, W. (2014). Battery Model for Crash Safety Simulations. Automotive Battery Technology, 19-35.

[9] Lowe, M., Tokuoka, S., Trigg, T., & Gereffi, G. (2010, October 5). Batteries For Electric Vehicles: The U.S. Value Chain. Center On Globalization Governance & Competitiveness, 1-76.

[10] Larsson, Fredrik, Andersson, Petra, & Mellander, Bengt-Erik. (2016). Lithium-Ion Battery Aspects on Fires in Electrified Vehicles on the Basis of Experimental Abuse Tests. *Batteries, 2*(9), 1-13.

[11] Avdeev, I., Martinsen, M., & Francis, A. (2014). Rate- and Temperature-Dependent Material Behavior of a Multilayer Polymer Battery Separator. *Journal Of Materials Engineering And Performance, 23*(1), 315-325.

[12] Perez, R. A. (1985). The Complete Battery Book (1st ed.). Blue Ridge Summit, PA: Tab Books.

[13] Zhang, S. (2007). A review on the separators of liquid electrolyte Li-ion batteries. *Journal of Power Sources,164*(1), 351-364.

[14] Arora, P., & Zhang, Z. (2004). Battery separators. *Chemical Reviews, 104*(10), 4419-4462.

[15] Huang, X. (2011). Separator technologies for lithium-ion batteries. *Journal of Solid State Electrochemistry, 15*(4), 649-662.

[16] Avdeev, I., Martinsen, M., & Francis, A. (2014). Rate- and Temperature-Dependent Material Behavior of a Multilayer Polymer Battery Separator. *Journal Of Materials Engineering And Performance, 23*(1), 315-325.

[17] Cannarella, J., Liu, X., Leng, C., Sinko, P., Gor, G., & Arnold, C. (2014). Mechanical Properties of a Battery Separator Under Compression and Tension. *Journal Of The Electrochemical Society, 161*(11), F3117-F3122.

[18] Gilaki, & Avdeev. (2016). Impact modeling of cylindrical lithium-ion battery cells: A heterogeneous approach. *Journal of Power Sources, 328*, 443-451.

[19] Yuan, S., & Chang, S. (2007). Texture Profile of Tofu as Affected by Instron Parameters and Sample Preparation, and Correlations of Instron Hardness and Springiness with Sensory Scores. *Journal of Food Science, 72*(2), S136-S145.

[20] Yoon, Jiyoung, Kim, Hyundeok, & Kim, Cheolhwan. (2015). Development of image error correction system for 3D optical microscope. *Computing Technology and Information Management (ICCTIM), 2015 Second International Conference on,*105-108.

[21] Abdullah, Bérubé, & Horne. (2014). SEM imaging of membranes: Importance of sample preparation and imaging parameters. *Journal of Membrane Science, 463*, 113-125.

[22] Kaufmann, Loser, & Leemann. (2009). Analysis of cement-bonded materials by multi-cycle mercury intrusion and nitrogen sorption. *Journal of Colloid And Interface Science, 336*(2), 730-737.

[23] Djian, Alloin, Martinet, Lignier, & Sanchez. (2007). Lithium-ion batteries with high charge rate capacity: Influence of the porous separator. *Journal of Power Sources, 172*(1), 416-421.

[24] Song, Jongchan, Ryou, Myung-Hyun, Son, Bongki, Lee, Je-Nam, Lee, Dong Jin, Lee, Yong Min, . . . Park, Jung-Ki. (2012). Co-polyimide-coated polyethylene separators for enhanced thermal stability of lithium ion batteries. *Electrochimica Acta, 85*, 524-530.

[25] Ryou, Mh, Lee, Dj, Lee, Jn, Lee, Ym, Park, Jk, & Choi, JW. (2012). Excellent Cycle Life of Lithium-Metal Anodes in Lithium-Ion Batteries with Mussel-Inspired Polydopamine-Coated Separators. *Advanced Energy Materials, 2*(6), 645-650.

[26] Wang, B., Richardson, T., & Chen, G. (2013). Stable and high-rate overcharge protection for rechargeable lithium batteries. *Physical Chemistry Chemical Physics,15*(18), 6849-6855.

[27] Fang, Ramadass, & Zhang. (2014). Study of internal short in a Li-ion cell-II. Numerical investigation using a 3D electrochemical-thermal model. *Journal of Power Sources, 248*, 1090-1098.

[28] Sahraei, Meier, & Wierzbicki. (2014). Characterizing and modeling mechanical properties and onset of short circuit for three types of lithium-ion pouch cells. *Journal of Power Sources, 247*, 503-516.

[29] Ramadass, Fang, & Zhang. (2014). Study of internal short in a Li-ion cell I. Test method development using infra-red imaging technique. *Journal of Power Sources,248*, 769-776.

[30] Lamb, & Orendorff. (2014). Evaluation of mechanical abuse techniques in lithium ion batteries. *Journal of Power Sources, 247*, 189-196.

[31] Kim, Cheon-Soo, Yoo, Jin-Seong, Jeong, Kyung-Min, Kim, Keon, & Yi, Cheol-Woo. (2015). Investigation on internal short circuits of lithium polymer batteries with a ceramic-coated separator during nail penetration. *Journal of Power Sources, 289*, 41-49.

[32] Santhanagopalan, Ramadass, & Zhang. (2009). Analysis of internal short-circuit in a lithium ion cell. *Journal of Power Sources, 194*(1), 550-557.

[33] Sheidaei, Xiao, Huang, & Hitt. (2011). Mechanical behavior of a battery separator in electrolyte solutions. *Journal of Power Sources, 196*(20), 8728-8734.

[34] Xia, Li, Ren, Gao, & Wang. (2014). Failure analysis of pinch–torsion tests as a thermal runaway risk evaluation method of Li-ion cells. *Journal of Power Sources, 265*, 356-362.

[35] Avdeev, & Gilaki. (2014). Structural analysis and experimental characterization of cylindrical lithium-ion battery cells subject to lateral impact. *Journal of Power Sources, 271*, 382-391.

[36] Doughty, D., Crafts, C., & United States. Department Of Energy. (2006). FreedomCAR :electrical energy storage system abuse test manual for electric and hybrid electric vehicle applications.

[37] Kalnaus, Wang, & Turner. (2017). Mechanical behavior and failure mechanisms of Li-ion battery separators. *Journal of Power Sources, 348*, 255-263.

[38] Naoe, Yamaguchi, & Futakawa. (2012). Quantification of fatigue crack propagation of an austenitic stainless steel in mercury embrittlement. *Journal of Nuclear Materials, 431*(1-3), 133-139.

[39] Li, S., Chen, C., Camardese, J., & Dahn, J. (2013). High Precision Coulometry Study of LiNi0.5Mn1.5O4/Li Coin Cells. *Journal Of The Electrochemical Society, 160*(9), A1517-A1523.

[40] Donal P. Finegan, Mario Scheel, James B. Robinson, Bernhard Tjaden, Ian Hunt, Thomas J. Mason, . . . Paul R. Shearing. (2015). In-operando high-speed tomography of lithium-ion batteries during thermal runaway. *Nature Communications, 6*(888), 6924.

[41] Sahraei, Hill, & Wierzbicki. (2011). Calibration and Finite Element Simulation of Pouch Li-ion Batteries for Mechanical Integrity. *Journal of Power Sources,* Journal of Power Sources.

[42] Kim, Yi, Shin, Han, & Park. (2011). Modelling the thermal behaviour of a lithium-ion battery during charge. *Journal of Power Sources, 196*(11), 5115-5121.